DANISH METEOROLOGICAL INSTITUTE

——— TECHNICAL REPORT ———

02-05

The operational DMI-HIRLAM system 2002-version

**Bent Hansen Sass, Niels Woetmann Nielsen,
Jess U. Jørgensen, Bjarne Amstrup
Maryanne Kmit and Kristian S. Mogensen**

COPENHAGEN 2002

ISSN: 0906-897X (printed version)
1399-1388 (online version)

The Operational DMI-HIRLAM System

Bent H. Sass, Niels W. Nielsen, Jess U. Jørgensen,
Bjarne Amstrup, Maryanne Kmit and Kristian S. Mogensen

Danish Meteorological Institute

Contents

1 Introduction **3**

2 Model dynamics **4**

2.1 The continuous equations 5

2.2 Semi-implicit scheme 7

2.3 Horizontal diffusion 8

2.4 Lateral boundary condition 8

2.5 Time filter 8

2.6 Time stepping 9

3 Physics **12**

3.1 Radiation 14

3.1.1 Shortwave radiation 15

3.1.2 Longwave radiation 17

3.2 Turbulence 19

3.2.1 Equations 19

3.2.2 Numerical aspects 21

3.3 Convection and condensation 22

4 Surface treatment **26**

4.1 Fluxes of momentum, heat and moisture at the surface 26

4.2 Surface energy and moisture budget 30

4.2.1 Equations for soil variables 30

4.2.2 Numerical aspects 31

4.3 Physiographic data 32

5 Data assimilation **32**

5.1 Minimization in 3D-Var 32

5.2 The observation handling system 34

6 Diagnostic output **35**

6.1 Wind at 10 metre 36

6.2 Temperature and humidity at 2 metre 36

6.3 Boundary layer height 37

6.4 MSLP 37

6.5 Diagnostic cloud cover 38

6.6 Visibility 38

6.7 Wind gusts 39

6.8 Icing index for aircraft 39

Appendix A DMI model setup (April 2002) **41**

Appendix B Grid used for horizontal discretization **47**

Appendix B.1 Vertical coordinate levels 47

Appendix C Computational details of longwave radiation **48**

1. Introduction

The numerical weather prediction system "DMI-HIRLAM" is run operationally at the Danish Meteorological Institute (DMI). The goal of the DMI weather prediction system is to provide high accuracy meteorological forecast products, with a special priority on forecasts valid for the short range, up to about two days ahead. The system provides guidance to both meteorological staff (forecasters) and to numerous customers in general. Furthermore, the results are used as input (forcing) to specialized forecasts (e.g., a storm surge model , an ocean wave model (WAM), and a road conditions model).

HIRLAM stands for HIgh Resolution Limited Area Model. This implies that the physical laws of the atmosphere expressed in mathematical form are transformed to numerical schemes operating on a system of grid points resolving the 3-dimensional space in high resolution, that is, with a short geographical distance between the model grid points. The model forecasts are carried out on a large computer system.

The DMI operational forecasting system originates from the international HIRLAM project (Machenhauer, 1988; Gustafsson, 1993; Källén, 1996; Undén et al., 2002). This collaboration started back in 1985 and has continued since then. The national meteorological institutes of Sweden, Spain, Norway, Ireland, Iceland, Holland, Finland and Denmark participate in the development of the forecasting system. Since 1992 Météo-France has been an associated partner. Although most components in the operational forecasting systems come from the international collaboration the implementations differ among the HIRLAM countries because of differences in areal coverage, computer facilities and various technical strategies chosen. The first HIRLAM based model at DMI became operational in October 1990.

The current operational DMI system (April 2002) involves several nested models and large integration domains (see Appendix A). The biggest HIRLAM model area needs boundary values evolving in time from an external model (the host model). In this case the host model is operated by the ECMWF (European Centre for Medium-Range Weather Forecasts). The inner models, in turn, receive their boundary values from the associated HIRLAM host model. The model forecasts need to start from realistic initial states of the atmosphere. This requires the processing of observations in a suitable data-assimilation system. The success of a numerical weather prediction system is governed by the quality of the forecast model in combination with the methodology for assimilating observations.

The main priority of the present report is to document the physical principles and the mathematical equations behind the DMI-HIRLAM forecast model. Numerical aspects of the model are included to some extent. Technical implementation details related to computers and model codes are not covered by the present report.

The model dynamics are described in section 2. This description concerns not only the continuous equations for atmospheric motion, but also numerical aspects including the question of coupling the model adiabatic processes with the diabatic processes (physical parameterizations). Information on the model grid used for the numerical computations is given in Appendix B.

The atmospheric physics are described in section 3. The key processes (radiation, turbulence, condensation and convection with precipitation release) are described, including also a description of parameterization problems associated with each process. Appendix C contains information on some details in the model computation of atmospheric longwave radiation.

The surface treatment is covered by section 4. At first, a description of the surface fluxes of heat, moisture and momentum over different surface types is provided. Secondly, the surface energy and moisture budget is described including prediction equations for soil variables. Finally, the generation of physiographic data is mentioned. These data provide the necessary information to assess the lower atmospheric boundary condition.

The system for assimilating observational data (the analysis system) is briefly outlined in section 5. The operational use of the data assimilation system is described in Appendix A, which contains information on operational data processing, geographical areas for the different model versions, and a table with key parameters of the operational setup.

Finally, important diagnostic measures of practical significance are described in section 6.

2. Model dynamics

From a physical and a mathematical point of view the behavior of the atmosphere is governed by the equations of motion, the equation of continuity for atmospheric constituents including moisture variables, the equation of state and the first law of thermodynamics. In addition, for the present hydrostatic model, the hydrostatic relation between increments of geopotential and pressure is utilized. The equations should include forcing terms comprising sources and sinks. Also the appropriate boundary conditions must be specified. For a Limited Area Model not only the lower and the upper boundary conditions are needed but also the lateral boundary conditions. The continuous equations are described in section 2.1.

In formulating a numerical model many considerations are needed on how to solve the atmospheric modeling problem. This is because the equations of motion allow for a rich variety of phenomena, and the numerical schemes used are crucially important for the quality and success of the model.

The present model dynamics are based on finite differences. The model grid (horizontal) is shown in Appendix B. The dynamics is of Eulerian type. In order to allow for reasonably long time steps the computations are split into an 'explicit part' and a 'semi-implicit part' (subsection 2.2). The latter takes care of the fast gravity wave terms such that the numerical stability criterion is governed by the meteorologically significant advection (CFL criterion).

In order to prevent accumulation of energy of the smallest scales a horizontal diffusion is required. For the current model resolutions this is utilized mainly for numerical reasons. Only for a very high resolution, resolving partly the turbulence, the horizontal diffusion will represent effects of horizontal turbulence. The horizontal diffusion currently used in HIRLAM is briefly described in subsection 2.3.

The lateral boundary condition represents a dynamical forcing which needs to be treated in a realistic way. The current methodology (boundary relaxation) is described in subsection 2.4. Three time levels of the forecast variables are available, and the time stepping is done by the *leapfrog* method (Haltiner, 1971). A time filter connecting even and odd time steps is described in subsection 2.5. The complete time stepping strategy including also the physical parameterizations is described in subsection 2.6. The model formulation allows for different time steps used for the dynamical processes and the physical parameterizations, respectively.

2.1. The continuous equations

The dynamical equations are solved for a general pressure based and terrain following coordinate $\eta(p, p_s)$. p is pressure and p_s is the surface pressure

$$\eta(0, p_s) = 0$$

and

$$\eta(p_s, p_s) = 1$$

The model is derived for a spherical coordinate system (λ, θ), but in the formulation two metric coefficients h_x, h_y have been introduced. For a distance $\delta X, \delta Y$ on the earth, with radius a, this yields

$$\delta X = a h_x \delta x$$

and

$$\delta Y = a h_y \delta y$$

Currently the HIRLAM model uses spherical rotated coordinates giving

$$\delta X = a \cos\theta \cdot \delta\lambda$$

and

$$\delta Y = a \delta\theta$$

The atmospheric forecast variables defined in three dimensions are the horizontal wind components u and v, surface pressure p_s, temperature T, specific humidity q, specific cloud condensate q_c and turbulent kinetic energy E. In the equations below, the forcing term for variable γ due to other processes than dynamics is called F_γ. The lateral boundary conditions are disregarded at this stage.

The momentum equations are

$$\frac{\partial u}{\partial t} = (f + \xi)v - \dot{\eta}\frac{\partial u}{\partial \eta} - \frac{R_d T_v}{a h_x}\frac{\partial \ln(p)}{\partial x} - \frac{1}{a h_x}\frac{\partial(\phi + E_m)}{\partial x} + F_u \qquad (1)$$

$$\frac{\partial v}{\partial t} = -(f + \xi)u - \dot{\eta}\frac{\partial v}{\partial \eta} - \frac{R_d T_v}{a h_y}\frac{\partial \ln(p)}{\partial y} - \frac{1}{a h_y}\frac{\partial(\phi + E_m)}{\partial y} + F_v \qquad (2)$$

In (1) and (2) above

$$\xi = \frac{1}{ah_xh_y}\left(\frac{\partial(h_yv)}{\partial x} - \frac{\partial(h_xu)}{\partial y}\right)$$

and

$$E_m = \tfrac{1}{2}(u^2 + v^2)$$

$\dot{\eta}$ is the vertical velocity in the η-coordinate system, ϕ is the geopotential, ξ is the vorticity and E_m is the kinetic energy of the mean horizontal motion (turbulent kinetic energy is E).

For temperature the equation is

$$\frac{\partial T}{\partial t} = -\frac{u}{ah_x}\frac{\partial T}{\partial x} - \frac{v}{ah_y}\frac{\partial T}{\partial y} - \dot{\eta}\frac{\partial T}{\partial \eta} + \frac{\kappa T_v \omega}{(1-(\delta_c-1)q)p} + F_T \tag{3}$$

κ is the ratio between the specific gas constant and the specific heat capacity, and δ_c is the ratio between the specific heat capacity of water vapor and the corresponding value of dry air (at constant pressure). ω is the rate of pressure change following an air parcel.

For the remaining variables ($\gamma = q$, $\gamma = q_c$ and $\gamma = E$) the following advection equation applies

$$\frac{\partial \gamma}{\partial t} = -\frac{u}{ah_x}\frac{\partial \gamma}{\partial x} - \frac{v}{ah_y}\frac{\partial \gamma}{\partial y} - \dot{\eta}\frac{\partial \gamma}{\partial \eta} + F_\gamma \tag{4}$$

The hydrostatic equation takes the form

$$\frac{\partial \phi}{\partial \eta} = -\frac{R_d T_v}{p}\frac{\partial p}{\partial \eta} \tag{5}$$

and the equation of continuity is

$$\frac{\partial}{\partial \eta}\frac{\partial p}{\partial t} + \nabla\cdot\left(\vec{v}_h\frac{\partial p}{\partial \eta}\right) + \frac{\partial}{\partial \eta}\left(\dot{\eta}\frac{\partial p}{\partial \eta}\right) = 0 \tag{6}$$

The definition of the divergence operator is

$$\nabla\cdot\vec{v}_h = \frac{1}{ah_xh_y}\left(\frac{\partial}{\partial x}(h_yu) + \frac{\partial}{\partial y}(h_xv)\right) \tag{7}$$

By integrating the equation of continuity using the boundary conditions $\dot{\eta} = 0$ at $\eta = 0$ and $\eta = 1$ the equation for surface pressure tendency is obtained

$$\frac{\partial p_s}{\partial t} = -\int_0^1 \nabla\cdot\left(\vec{v}_h\frac{\partial p}{\partial \eta}\right) d\eta \tag{8}$$

The equation for pressure vertical velocity is

$$\omega = \frac{\partial p_s}{\partial t} + \int_\eta^1 \nabla\cdot\left(\vec{v}_h\frac{\partial p}{\partial \eta}\right) d\eta + \vec{v}_h\cdot\nabla p \tag{9}$$

and the equation for $\dot{\eta}$

$$\dot{\eta}\frac{\partial p}{\partial \eta} = \left(1 - \frac{\partial p}{\partial p_s}\right)\frac{\partial p_s}{\partial t} + \int_\eta^1 \nabla\cdot\left(\vec{v}_h\frac{\partial p}{\partial \eta}\right) d\eta \tag{10}$$

2.2. Semi-implicit scheme

A description of the finite difference form of the adiabatic equations above has been made (Källén, 1996), see also (Simmons and Burridge, 1981). Following the work of (Arakawa, 1966) and (Sadourny, 1975), the scheme has been designed to preserve, in a global model, several important integral constraints associated with the continuous equations, e.g., the conservation of mass.

The pressure at the coordinate surfaces (half levels) are given from the following expression using predefined coefficients $A_{k+\frac{1}{2}}$ and $B_{k+\frac{1}{2}}$, $(k = 0, \ldots, N)$, where:

$$p_{k+\frac{1}{2}} = A_{k+\frac{1}{2}} + B_{k+\frac{1}{2}} p_s \tag{11}$$

In (11) the coefficients $A_{k+\frac{1}{2}}$ and $B_{k+\frac{1}{2}}$ are currently chosen such that $B_{k+\frac{1}{2}} = 0$ for the uppermost levels (pressure coordinate surfaces) while $A_{k+\frac{1}{2}} = 0$ near the ground (terrain following coordinates). The finite differences are second order accurate and the horizontal grid is an Arakawa C grid (see Appendix B).

For specific humidity q, cloud condensate q_c and subgrid scale kinetic energy E an upstream advection scheme has been implemented in 3 dimensions in order to improve advection characteristics compared to centered difference numerics. The remaining forecast variables are subject to semi-implicit corrections as described below. The preliminary updates from the dynamics are written in the following form using a *leapfrog* time step

$$u^*_{n+1} = u_{n-1} + 2\Delta t \left(\frac{\partial u}{\partial t}\right)_{e,n} - \frac{1}{a h_x}\delta_x \left(\tfrac{1}{2}\Delta_{tt} P\right) \tag{12}$$

$$v^*_{n+1} = v_{n-1} + 2\Delta t \left(\frac{\partial v}{\partial t}\right)_{e,n} - \frac{1}{a h_y}\delta_y \left(\tfrac{1}{2}\Delta_{tt} P\right) \tag{13}$$

$$T^*_{n+1} = T_{n-1} + 2\Delta t \left(\frac{\partial T}{\partial t}\right)_{e,n} - \tfrac{1}{2}\tau \Delta_{tt} d \tag{14}$$

$$\ln p^*_{s,n+1} = \ln p_{s,n-1} + 2\Delta t \left(\frac{\partial \ln p_s}{\partial t}\right)_{e,n} - \tfrac{1}{2}\nu \Delta_{tt} d \tag{15}$$

In the equations above the first term on the right hand side is the prognostic variable at the old time step, the second term is an explicit term using the dynamical equations described in the previous section. The third term of each equation is a semi-implicit term included to treat gravity wave terms in such a way that the time step allowed to retain numerical stability in the model is determined by the advection terms. Let γ be an arbitrary parameter. The following definitions apply:

$$\delta_t(\gamma) = \frac{(\gamma_{n+1} - \gamma_{n-1})}{2\Delta t}$$

$$P = \chi T + R_d T_r \ln p_s$$

$$d = \nabla \cdot \vec{v}_k$$

The matrices χ, τ and ν include constants in the vertical discretization. A linearization is done about a constant reference temperature T_r and surface pressure p_r. Further details of the semi-implicit scheme have been documented, (Källén, 1996). No semi-implicit corrections are used for (q, q_c and E).

2.3. Horizontal diffusion

A linear fourth order horizontal diffusion scheme is applied on the preliminary updated values of the forecast parameters after the explicit and the semi-implicit updates. The increment $\delta\gamma_{hd}$ to the preliminary updated values γ^*_{n+1} are

$$\delta\gamma_{hd} = \gamma^*_{n+1} - \Delta t K_\gamma \nabla^4 \gamma^*_{n+1} \tag{16}$$

K_γ is a diffusion coefficient depending on resolution and time step. For details see (Källén, 1996). Currently no horizontal diffusion is used for q, q_c and E.

2.4. Lateral boundary condition

A Limited Area Model (LAM) is dependent on the forcing of the atmospheric forecast variables from the boundary conditions supplied by a host model. A distinction is made between variables supplied by the host model and variables only available in the LAM. The former type of variables are u, v, T, q and $\ln p_s$. For these variables the interior variables are adjusted towards the prescribed boundary values γ_b as a further update to the preliminary values γ^*_{n+1} at the new time step. A similar boundary relaxation strategy has been described (Davies, 1976; Kållberg, 1977).

$$\gamma_{n+1} = (1 - \alpha_b)\gamma^*_{n+1} + \alpha_b \gamma_{b,n+1} \tag{17}$$

In (17) γ_b is linearly interpolated in time between boundary data sets. The boundary update frequency (new values for time interpolation) and further details concerning boundary data in an operational context, are given in Appendix A for the different operational HIRLAM versions. The default value of α_b is

$$\alpha_b = 1 - \tanh\left(j\frac{2}{M-4}\right) \tag{18}$$

where j is the number of grid points from the boundary point and M is the width of the boundary zone.

The variables currently not supplied by the ECMWF model to the large scale operational DMI-HIRLAM-G model (see Appendix A) are q_c and E. In order not to impose unrealistic values inconsistent with the interior model, a relaxation similar to that described above is applied to dynamical tendencies of the forecast variables in the boundary zone. The implementation is such that the dynamical tendency produced at the boundary is having zero weight while full weight is assigned to the inner edge of the boundary zone. On the boundary points these variables evolve as a result of the physical parameterizations only.

2.5. Time filter

Three time levels of the forecast variables are available and the time stepping is done by the *leapfrog* method (subsection 2.2). In order to suppress a possible separation of even

and odd time steps when using *leapfrog* time stepping the following simple time filter is used for the forecast variable γ

$$\gamma_{fil,n} = \gamma_n + \epsilon_{fil}(\gamma_{fil,n-1} + \gamma_{n+1} - 2\gamma_n) \tag{19}$$

In the equation (19) above index 'fil' means a time filtered value. The time filter constant ϵ_{fil} is currently 0.05.

2.6. Time stepping

A procedure for including the forcing terms from the physical parameterizations (see section 3) have not yet been described. Experimentation with the HIRLAM system shows that the method used to couple updates from dynamics and physics, respectively, is important with regard to the control of numerical noise. Also the numerical stability may be affected by the coupling method. This is because the physics and dynamics may interact strongly on the smallest scales treated by the model. The importance of the coupling has also been found in other model systems (Wedi, 1999a; Wedi, 1999b).

The time stepping described below has lead to an improved numerical stability of high resolution forecasts, a better control of numerical noise and considerable savings in computer time. The time stepping is illustrated in fig. 1 and fig. 2.

The physics and dynamics operate with different time steps. The length of a physics time step is Δt_P which is N_P times the dynamical time step Δt. The effects of the physical parameterizations operating in a vertical column are added only every N_P time step to a model state developed as a result of model dynamics. With Eulerian dynamics N_P may be an integer exceeding 10 for a high resolution model. The time stepping may also be used in a semi-Lagrangian framework using a correspondingly smaller number of N_P. Operationally Eulerian dynamics is used with $N_P = 6$ for models 'E', 'N' and 'D'. $N_P = 3$ for model 'G' (See Appendix A). The processing proceeds according to the following steps:

1) A complete model state is saved for the physics computations.

2) The model is run without physics (adiabatic model dynamics) for N_P time steps using the *leapfrog* time stepping. Also the horizontal diffusion (linear fourth order), the boundary relaxation and the time filter is applied every dynamical time step Δt which is finalized by a swapping (renaming) of variables for the next time step. After N_P time steps the effect of the physical parameterizations over the physics time step is to be added.

3) The input to the physics computations is the old model state mentioned in 1) Dynamical tendencies are needed for the turbulence- and convection parameterization. These tendencies are obtained as the difference between the preliminary model state $\gamma^I_{n+N_P}$ and γ_n for variable γ (adiabatic process difference). Then the physics are computed and the increment over N_P time steps is supplied as an update to the preliminary values at time steps $n - 1 + N_P$ and $n + N_P$, in order to make continued time stepping cycles possible.

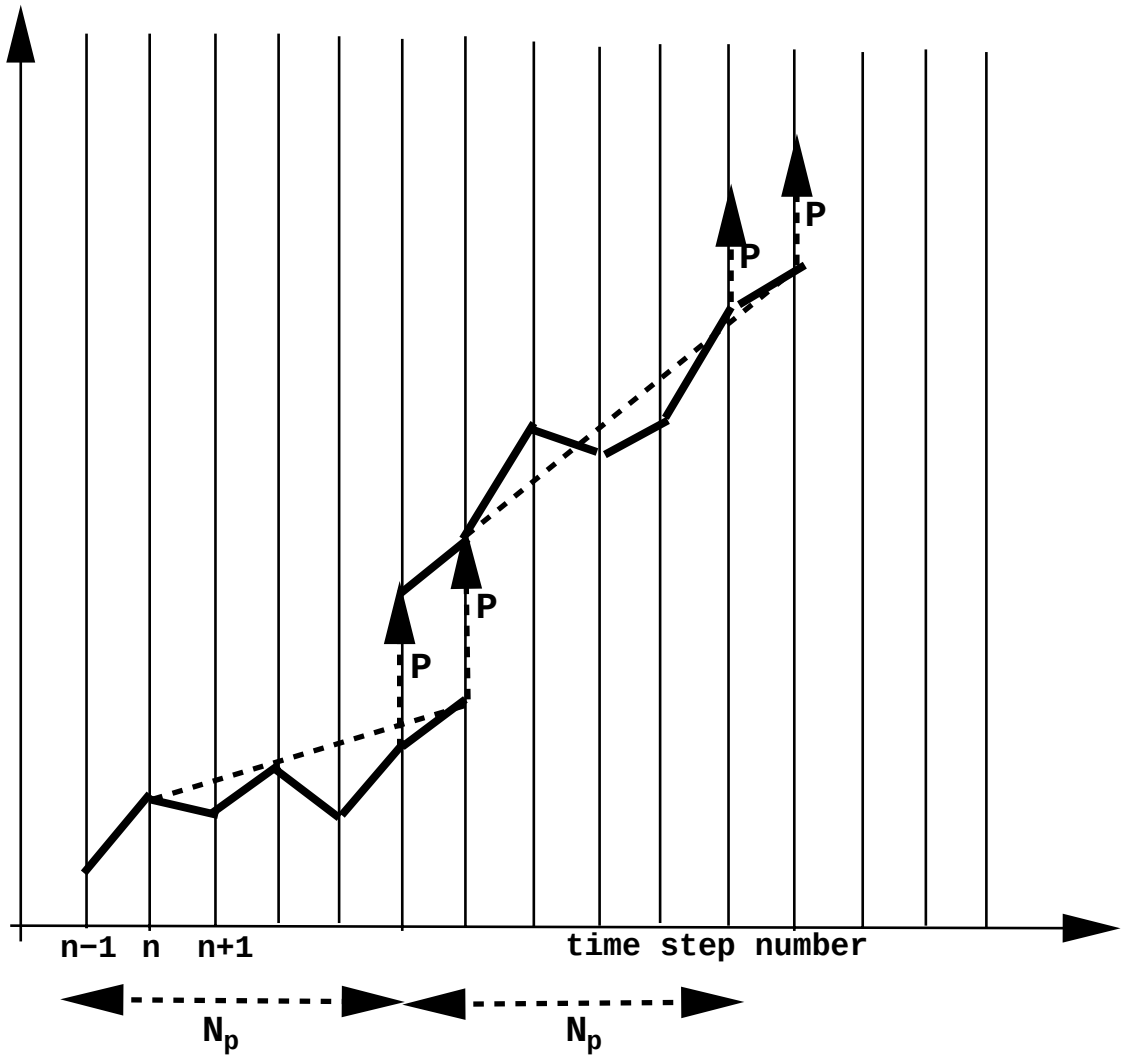

Figure 1: Time stepping cycle, vertical dashed arrows "P" represent the adding of physics increments valid for past N_P time steps.

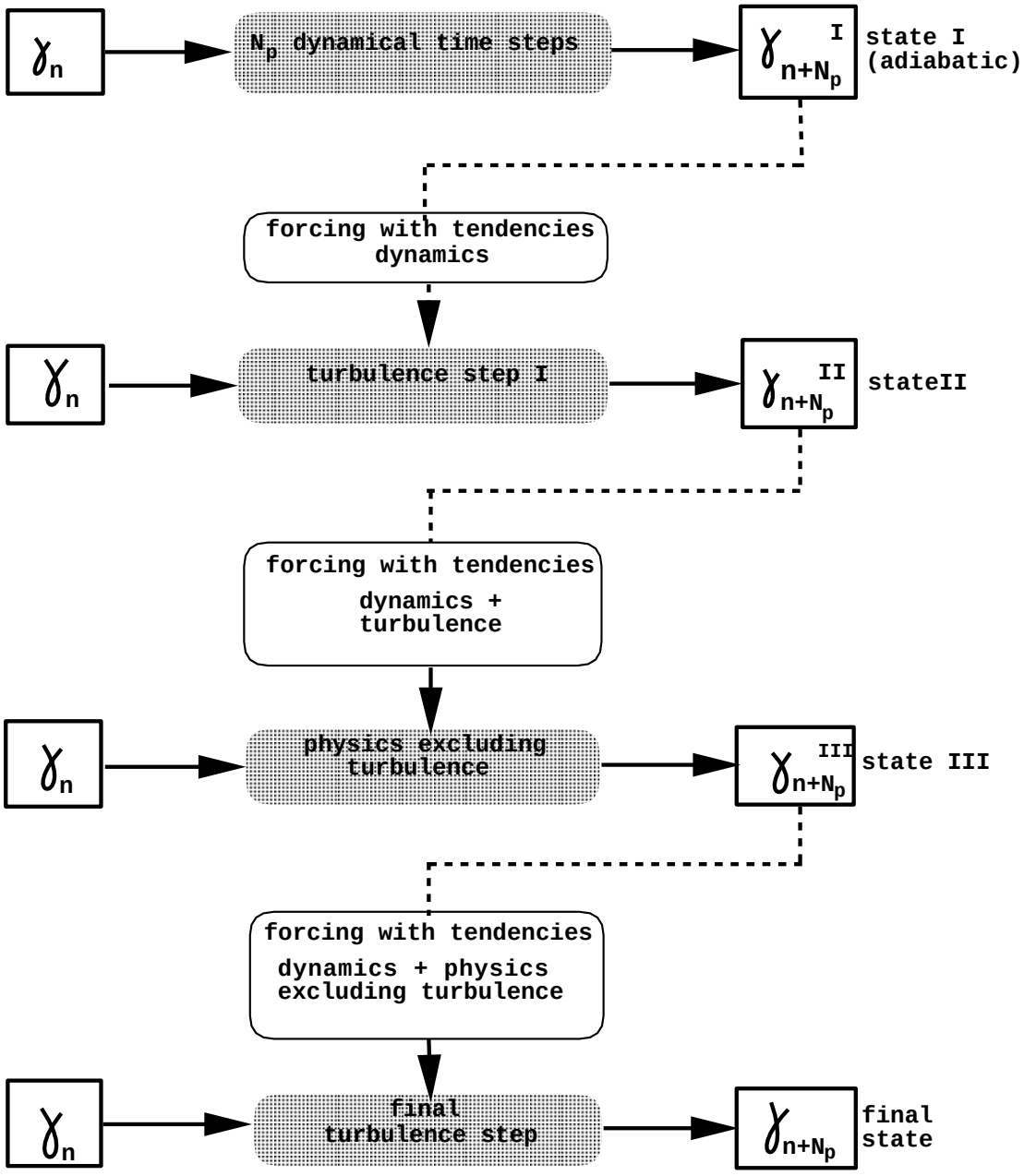

Figure 2: Iterative steps in physics computations (see text).

4) The time stepping described above has been further upgraded (September 2000). The idea is to let a process 'know' about other processes acting simultaneously. This principle has been adopted when computing the turbulence processes and is in particular important when using large time steps. The turbulence computation is treated twice in an iterative solution of the physics contribution. The first computation is needed for the convection parameterization.

$$\frac{(\gamma_{(P_{tur}+D)} - \gamma_n)}{\Delta t_P} = F_\gamma + D_\gamma + P_\gamma \tag{20}$$

In (20) $\gamma_{(P_{tur}+D)} = \gamma^{II}_{n+N_p}$ signifies an update due to turbulence and dynamics processes and γ_n is the model variable at time level n. On the right hand side of (20) F_γ expresses an implicit non-linear relationship associated with the turbulence scheme. Other model variables than γ are involved, consisting of known values during the solution of the equation for γ. D_γ is the known time averaged source term from dynamics. P_γ is the source term due to a precomputed surface flux. The solution of (20) is a tridiagonal solver. The source term due to dynamics needs to be subtracted afterwards to get the tendency contribution from turbulence alone. The latter is needed when making the second call to the turbulence scheme, as described below.

After computing the rest of the physical processes we add all model process tendencies to form another preliminary model state $\gamma^{III}_{n+N_P}$ (see fig. 2). The total model tendency is so far

$$\frac{(\gamma^{III}_{n+N_P} - \gamma_n)}{\Delta t_P} \tag{21}$$

A final step is then made where the turbulence process is computed with the dynamics and all other physics contributions than turbulence as source terms. This total forcing can be obtained by subtracting the saved turbulence tendency of the first call to the turbulence scheme from the total model change in (21).

The final computation with dynamics (D) and physics (P) included is given by

$$\frac{(\gamma_{(P+D)} - \gamma_n)}{\Delta t_P} = F_\gamma + D_\gamma + P'_\gamma \tag{22}$$

In (22) the source term P'_γ includes also the effect of a recomputed surface flux valid at the middle of the physics time step. The new model state is

$$\gamma_{(n+N_P)} = \gamma_n + (\gamma_{(P+D)} - \gamma_n) = \gamma_{(P+D)}$$

3. Physics

The role of physical parameterizations in an atmospheric model is to describe diabatic effects. In addition, the physics are necessary in order to obtain predictions of weather parameters such as rain and clouds. The physics comprise the processes of radiation and subgrid scale transports of momentum, temperature and moisture variables down to small scales associated with turbulence. In addition, the thermodynamics associated

with latent heat release (e.g., condensation, evaporation, sublimation and precipitation) must also be described. The boundary conditions at the ground need also to be taken into account.

Parameterization of subgrid scale phenomena depends on the resolution of the model, because resolution defines an ability to resolve a given phenomenon. A simple example is the parameterization of cloud cover. In large scale models a stratiform cloud cover is often parameterized as a function of relative humidity, starting to become nonzero at a threshold relative humidity much below 100 percent, in order to account for subgrid scale variability of moisture. As the model resolution increases it is obviously not realistic to retain the cloud cover threshold at a fixed value, since the subgrid scale variability must decrease as the resolution becomes increasingly high.

It may therefore be concluded that physical parameterizations should depend on the resolution of the atmospheric model. As the model mesh size used in HIRLAM covers a range from that of a large scale model (around 50 km) to a size of about 5 km, it is to be expected that some adjustment of parameterizations with resolution is important. Two strategies are possible here. One may choose to do some tuning which is often rather 'ad hoc' for a modified resolution. This practice has been widely used in atmospheric modeling due to the lack of precise knowledge about a correct resolution dependence of physics.

Another approach is to realize that physics should be scale dependent and to formulate mathematical expressions for such dependencies, based on reasonable estimates for high and low resolutions. The latter approach has to some extent been applied in the formulation of condensation processes in the HIRLAM model (see subsection on clouds and condensation).

Each physical process has its own problems to address in high resolution. For radiation processes a challenging situation occurs at very high resolution since the transmission of radiation from neighboring grid boxes can contribute to the local heating rate. In addition, the local cloud cover in a vertical column will in some situations not provide accurate information when computing solar radiation at the ground. This is because slant beams may pass through neighboring grid boxes with differing cloud amounts. Also the slope of the ground exposed to direct solar radiation becomes locally significant at high resolution, implying increased spatial variability of solar energy flux to the ground as resolution increases. These phenomena which become of some importance at resolutions below 10 km have not yet been addressed in the HIRLAM physics. The emphasis has been on describing radiative processes with reasonable accuracy in the troposphere. A fast radiation scheme (Savijärvi, 1990) has been further developed for HIRLAM (Sass et al., 1994). The scheme is normally called with the same frequency as other physical processes. This allows for describing radiation associated with fluctuating cloud cover at short time scales.

The atmospheric subgrid scale transports of heat, moisture and momentum at traditional model resolutions are dominated by the vertical transports. These take place over a large range of spatial scales, from large convective scales to small scales associated with turbulence. The goal is to describe accurately the effect of all subgrid scales on the

resolved scales of motion. Traditionally these transports are separated into two scales, namely the small subgrid scales expressed by turbulence, and larger scales described by a convective parameterization. Due to the complexity of atmospheric states it is a challenge to make a coherent formulation of turbulence and convection parameterization.

In addition, the transports of moisture also has to describe phase changes. Therefore all processes connected to condensation and precipitation must be included. At increased model resolution more of the transports will be done by the resolved scale dynamics exposed to larger vertical velocities as a consequence of higher amplitude small scale convergence in the atmospheric flow. Hence the convection parameterization should accomplish less vertical moisture transports as the model resolution increases. A special problem associated with convection schemes is the break down at high resolution of the traditional assumption that convective cloud samples exist in balance with the synoptic forcing acting on the column of air above each grid square. There are indications (Emanuel, 1991) that convection needs to be parameterized at model resolutions below 10 km in order to take into account the very small scale convective updraft with high vertical velocities. However, the details on how to best incorporate a convection parameterization at a high model resolution (below 10 km) still appear to be an open question. The interaction of the model atmosphere with the ground takes place via complex processes of heat, moisture and momentum transfer. The surface processes are the boundary conditions for the vertical subgrid scale transports.

A special effect is created by subgrid scale orography exerting a gravity wave drag on the atmosphere. This effect which is considered important in synoptic scale models is currently not parameterized in HIRLAM. With increased model resolution this model limitation gradually diminishes. Currently the surface fluxes are described in terms of effective roughness lengths that may differ substantially for momentum, heat and moisture. The turbulent transports are communicated to the atmosphere by a diffusion scheme based on 'turbulent kinetic energy' as a prognostic variable (Cuxart et al., 2000). The inclusion of this additional dependent model variable provides a better potential to describe the effect of turbulent processes as compared to simple first order schemes. One reason is that the 'memory' of turbulence may be advected by the resolved flow. This represents an additional way for physics and dynamics to interact.

The extremely inhomogeneous and complex lower boundary condition with huge spatial variations of the physical properties of the surface in some regions makes it very difficult to parameterize accurately the averaged surface fluxes of momentum, heat and moisture. The first steps have been taken to improve the description of the lower boundary conditions supplied by physiographic data. New databases are utilized, e.g., a Global data base from the U.S. Geological Survey (USGS) and a local data base (Sattler, 1999).

The individual physical parameterizations of HIRLAM are described below.

3.1. Radiation

The purpose of the radiation parameterization scheme is to provide fluxes as a result of both solar radiation and infrared (thermal) radiation throughout the atmosphere. The

temperature tendency providing the diabatic forcing to atmospheric motions may be written

$$\frac{\partial T}{\partial t} = -\frac{g}{c_p}\frac{\partial F_{net}}{\partial p}. \tag{23}$$

In (23) above T is temperature, t is time, g is the acceleration of gravity, c_p is the specific heat capacity of air at constant pressure, F_{net} is the integrated net radiation flux due to all significant wave lengths, and p is pressure.

The science behind radiation is in principle rather well understood. In practice, the computational demands required to carry out the so called 'line-by-line' calculations over the whole spectrum of interest are so extreme that such a strategy cannot be followed in a forecast model. Most forecast models perform radiative computations over rather few selected spectral intervals resolving the spectrum associated with solar radiation and thermal radiation.

The present radiation scheme treats radiation in a highly parameterized and simplified way. This allows for frequent calls to the radiation scheme such that, for example, the effect of changing cloud cover within short time scales can be accounted for. The fast radiation scheme (Savijärvi, 1990) developed for high resolution meso-scale models has been adopted. The scheme for parameterizing cloud effects has been developed further for HIRLAM purposes (Sass et al., 1994). The radiation scheme which is summarized below, does not attempt to explicitly resolve the radiation spectrum except for a separate treatment of 'solar radiation' and 'thermal radiation'.

3.1.1. Shortwave radiation

The temperature tendency $\left(\frac{\partial T}{\partial t}\right)_s$ due to absorption of solar radiation is formulated according to

$$\left(\frac{\partial T}{\partial t}\right)_s = \left(\frac{\partial T}{\partial t}\right)_{sa}(1 - f_M) + \left(\frac{\partial T}{\partial t}\right)_{sc} f_M \tag{24}$$

The first term on the right hand side represents absorption in clear air, and the second term absorption in cloudy air. As an approximation we consider the cloudy fraction f_M to be equal to the maximum fractional cloud cover of all levels in a vertical column. In this formulation it is assumed that the maximum cloud cover applies to all levels below the uppermost cloud layer. Hence the cloud water content valid for clouds in a given model layer is scaled by a factor of $\frac{f}{f_M}$. A cloud water content $q_c' = \frac{q_c}{f_M}$ inside the cloud will then guarantee consistency between vertically integrated cloud water from the grid box model variable q_c and the vertically integrated cloud water used for the cloudy part of the shortwave computation. Above the uppermost cloud level the solar heating equals the clear air contribution.

It is necessary to specify at a given time the top of the atmosphere (TOA) solar flux S and the solar zenith angle θ. These are computed according to well known formulae from the literature (Paltridge and Platt, 1976). The heating rate of the clear air is computed according to (25–28), (Savijärvi, 1990)

$$\left(\frac{\partial T}{\partial t}\right)_{sa} = S\frac{q}{c_p}\frac{p}{p_0}[Y(u_s) + b_1\alpha\cos\theta Y(u_*)] + b_2(\cos\theta)^{0.3} \tag{25}$$

$$Y(u_s) = \begin{cases} b_3 u_s^{-0.81}, & u_s \geq 0.05 \text{ cm} \\ b_4 u_s^{-0.63}, & u_s < 0.05 \text{ cm} \end{cases} \tag{26}$$

$$u_s = \frac{1}{\cos\theta} u_{(0,p)} \tag{27}$$

$$u_* = \frac{1}{\cos\theta} u_{(0,p_s)} + b_1 u_{(p,p_s)}. \tag{28}$$

where

$$u_{(p_1,p_2)} = \frac{1}{g} \int_{p_1}^{p_2} q \frac{p}{p_0} dp$$

and α is the shortwave albedo of the ground. u_s is the slant direct beam, i.e., vertically integrated water vapor path linearly scaled by pressure and divided by $\cos\theta$ (in cm). u_* is the path length for isotropically reflected beams and $p_0 = 1013$ hPa is a reference pressure. The values of the constants b_1 to b_4 are given in Appendix C.

The two terms of (25) in brackets represent the absorption by water vapor in the direct and in the surface reflected beams, respectively. They are based on comparisons with line-by-line calculations (Chou, 1986). The last term in (25) is a parameterization of absorption by CO_2, O_2 and O_3, based on the standard absorption curves (Sasamori et al., 1972) and average amounts of these absorbing gases in the troposphere.

The cloud absorption is given by

$$\left(\frac{\partial T}{\partial t}\right)_{sc} = \widehat{T}_{p_Z,p} \left(\frac{\partial T}{\partial t}\right)_{sa} + \frac{g}{c_p} F_{sZ} \frac{\partial}{\partial p} \widehat{A}_{(p_Z,p)}. \tag{29}$$

The total absorption is determined as the sum of the clear air absorption modified by the transmittance factor for the cloudy atmosphere (the first term) plus a major contribution from cloud drop absorption and increased path lengths due to scattering (the second term). $\widehat{A}$ and $\widehat{T}$ are, respectively, the absorptance and transmittance from the top of the uppermost cloud layer to a level below. F_{sZ} is the solar flux density at the top of the uppermost cloud layer. This flux density is parameterized according to (30), as given originally for clear sky conditions at the ground, with $p = p_s$ (Savijärvi, 1990).

$$F_{sZ} = S \cos\theta \left[1 - 0.024 \cos\theta^{-0.5} - b_5 \cdot 0.11 \cdot u_s^{0.25} - b_6 \frac{p}{p_{00}} \left(\frac{0.28}{1 + 6.43 \cos\theta} - 0.07\alpha_*\right)\right] \tag{30}$$

where $p_{00} = 1000$ hPa is a reference pressure. The first term in the brackets of (30) depending on the zenith angle θ concerns the stratospheric absorption due to ozone. A major contribution to the extinction of solar radiation comes from tropospheric absorption due to water vapor, CO_2 and O_2. This is parameterized according to the term involving u_s in (30). The last term involving two contributions describes the effect of scattering. The first contribution arises from scattering of the incoming solar beam while the second one is a compensating effect due to reflected radiation (from the cloud below having an albedo α_*), which is back-scattered from the atmosphere above. The coefficients, b_5 and b_6, if larger than 1 (see Appendix C), represent a crude inclusion of effects due to aerosol absorption and scattering, respectively.

In order to define cloud layer absorptance and transmittance, simple formulae have been fitted to approximate results obtained with more detailed multiple scattering schemes (Slingo et al., 1982; Stephens, 1978; Liou and Wittman, 1979), for stratus type of droplet distributions.

$$\widehat{A} = b_7(b_8 + \cos\theta)\ln(1 + b_9 M_t) \tag{31}$$

$$\widehat{T} = \frac{\widehat{T}_1}{(\widehat{T}_1 + M_t)}\,, \tag{32}$$

In (31) and (32) $\widehat{T}_1 = b_{10}(b_{11} + \cos\theta)$ and M_t is the vertically integrated cloud water content (in g/m^2) from the top of the uppermost cloud layer to a level below. Values of the constants b_7 to b_{11} are given in Appendix C. Finally, the net solar flux at the ground F_{s0} is computed according to (33) as a product of $(1-\alpha)$ and a weighted sum of a clear air contribution F_{s0a} determined from a formula similar to (30), plus a cloudy contribution F_{s0c} according to (34):

$$F_{s0} = (1-\alpha)[F_{s0a}(1 - f_M) + F_{s0c} f_M] \tag{33}$$

$$F_{s0c} = F_{sZ}\frac{\widehat{T}_{(p_Z,p_s)}}{1 - \alpha(1 - \widehat{T}_{(P_Z,P_s)})b_{12}} \tag{34}$$

The denominator in (34) takes into account multiple reflections between ground and cloud. The factor b_{12} accounts for absorption in reflected beams. This heating term, usually small, is included as a uniformly distributed heat source below the cloud top. Multiple reflections between two cloud layers are not explicitly included in the scheme.

3.1.2. Longwave radiation

The longwave scheme is based on an empirical emissivity function $e(p_{i-\frac{1}{2}}, p_{j+\frac{1}{2}})$ defined according to (35)

$$e(p_{i-\frac{1}{2}}, p_{j+\frac{1}{2}}) = a_1 + a_2 X - a_3 X^2 - a_4 X^3\,, \tag{35}$$

where

$$X = a_5 \ln\left(\sum_{k=i}^{j} q_k \frac{p_k}{p_{00}}\frac{\Delta p_k}{10g}\right)$$

The water vapor path has been scaled linearly with pressure. The values of the constants a_1 to a_5 are given in Appendix C. The clear air cooling rate based on (35) takes into account cooling due to water vapor line spectrum. It can be shown (Savijärvi, 1990) that the cooling rate may be written as a sum of three terms. One term expressing "local cooling to space" is usually significantly larger than are the other terms in the free atmosphere. A second term expressing interaction between the surface and the atmosphere is of significance close to the ground. A third term which determines the exchange of radiation with other layers is usually small and is neglected in clear sky calculations. Also a complete interaction between levels is avoided for the cloudy part of the computations. However, the significant effect of radiative interaction between clouds is retained as described in Appendix C. These simplifications may be defended

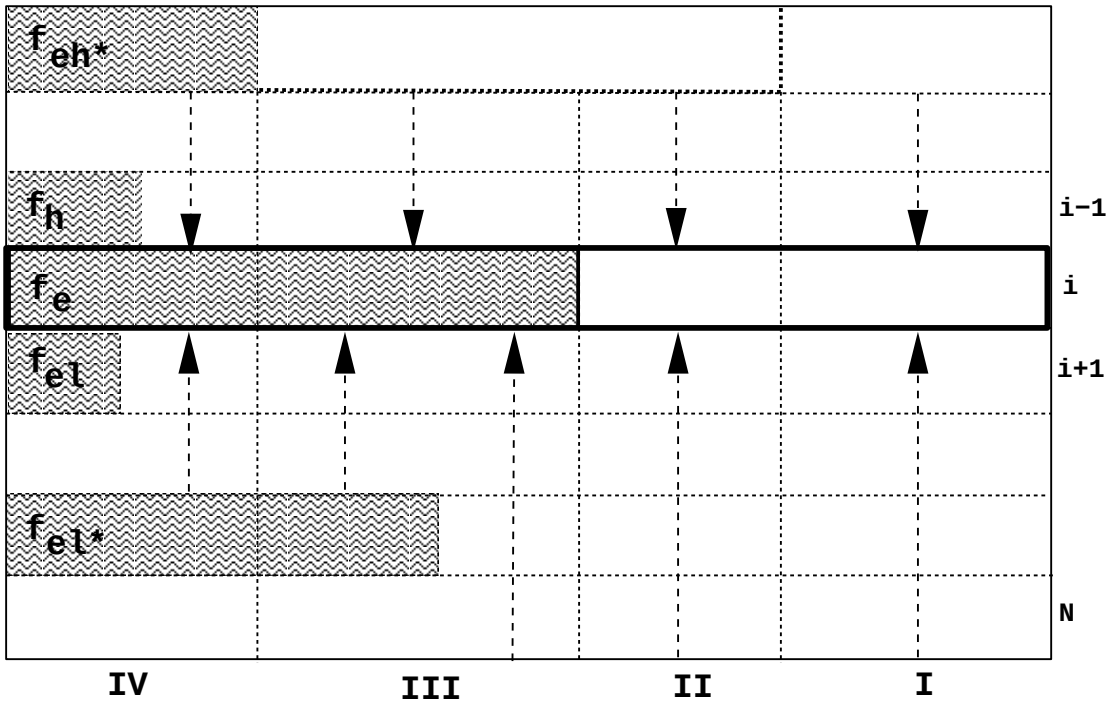

Figure 3: Computational scheme for infrared computations.

only with reference to computational efficiency which is increased since the number of calculations become proportional to the number of model levels, and not to the number of levels squared.

Formally, the computation of the radiative temperature tendency due to thermal radiation is split up into four parts

$$\left(\frac{\partial T}{\partial t}\right)_i = \left(\frac{\partial T}{\partial t}\right)_{i1a} + \left(\frac{\partial T}{\partial t}\right)_{i2a} + \left(\frac{\partial T}{\partial t}\right)_{i1c} + \left(\frac{\partial T}{\partial t}\right)_{i2c} \tag{36}$$

Each of the terms in (36) is a weighted contribution to the total tendency. The scheme applies to a maximum cloud overlap assumption. The first term (I) is the heating rate contribution from the clear air part of the grid box with no clouds above while the second term (II) is the clear air contribution with clouds above. Similarly, the third term (III) is the cloudy contribution without clouds above and the fourth term (IV) a contribution with clouds above. The cloud covers used in the computations are effective cloud covers where the customary assumption is made that "grey" clouds may be introduced by reducing the grid box fractional cloud cover f with the cloud emissivity. The computational details are given in Appendix C.

The downward surface flux from the clear atmosphere is obtained from (37). In addition to the summation of the contributions from all levels expressed by the Planck function $B(T_k)$ and the emissivity function (first term) three additional terms are added. The

first one (a_9) corresponds to the flux contribution due to aerosols. The last two terms are added to describe the effect of water vapor continuum.

$$F_{i0a} = \sum_{k=1}^{N} B(T_k) \cdot [e(p_{k-\frac{1}{2}}, p_s) - e(p_{k+\frac{1}{2}}, p_s)] + a_9 + a_{10}\sqrt{q_N} + a_{11} q_N. \tag{37}$$

Index N refers to the lowest model layer. The total downward flux from the atmosphere is obtained by adding a cloudy contribution F_{i0c} determined as radiation transmitted to the ground from an effective cloud cover according to the empirical expression in (38). The term in the square brackets is a fractional transmission estimated from the clear air contribution F_{i0a} and a low troposphere effective temperature T_{ef}

$$F_{i0c} = B(T_{h*}) f_{eh*}(N) \left[1 - \frac{F_{i0a}}{(\sigma T_{ef}^4)} \right] \tag{38}$$

$$T_{ef} = T_N - a_{15} \left(\frac{\partial T}{\partial p} \right)_N \tag{39}$$

The net radiation at the ground due to longwave radiation follows from (40)

$$F_{i0} = \varepsilon_0 (F_{i0a} + F_{i0c} - \sigma T_{e0}^4) \tag{40}$$

σ is the Stefan Boltzmann's constant and ε_0 is the emissivity of the surface taken to be 0.95.

3.2. Turbulence

Turbulent transport of moisture, sensible heat and momentum plays an important role in the atmosphere. The parameterization of turbulence in numerical models of the atmosphere is therefore of great concern. In recent years various turbulence schemes have been tested in HIRLAM. One such is a variant of the Louis scheme (Louis et al., 1982). In this scheme the vertical transports are based on local gradients of the forecast variables. A refined description of the unstable planetary boundary layer became available with a nonlocal first order scheme (Holtslag and Boville, 1993; Nielsen, 1998). Recently the turbulence processes have been formulated in the framework of a new prognostic forecast variable 'subgrid scale kinetic energy'. This variable does in principle describe all subgrid scale kinetic energy. The turbulence processes include the small scale motions while convection accounts for larger eddies. The scheme describing the turbulence transports (Cuxart et al., 2000) is briefly described below.

3.2.1. Equations

The effect of turbulence on the mean flow is approximated by

$$\partial \overline{u} / \partial t = -\partial [\overline{u'w'}]_{tur} / \partial z \,, \tag{41}$$

$$\partial\overline{v}/\partial t = -\partial[\overline{v'w'}]_{tur}/\partial z\,, \tag{42}$$

$$\partial\overline{\theta}/\partial t = -\partial[\overline{\theta'w'}]_{tur}/\partial z\,, \tag{43}$$

$$\partial\overline{q}/\partial t = -\partial[\overline{q'w'}]_{tur}/\partial z\,, \tag{44}$$

$$\partial\overline{q}_c/\partial t = -\partial[\overline{q'_c w'}]_{tur}/\partial z\,, \tag{45}$$

i.e. the horizontal derivatives of the second order covariance (Reynolds) terms are assumed to be much smaller than the vertical derivatives. θ is potential temperature in (43). Index *tur* stands for 'turbulence'. Note that specific cloud water (q_c) is included as a prognostic variable. To the same level of approximation the equation for subgrid scale kinetic energy takes the form

$$\begin{aligned}\frac{\partial\overline{E}}{\partial t} &= -\left[\overline{u'w'}\frac{\partial\overline{u}}{\partial z} + \overline{v'w'}\frac{\partial\overline{v}}{\partial z} + \overline{w'w'}\frac{\partial\overline{w}}{\partial z}\right] \\ &\quad + \left[\frac{g}{\overline{\theta}_v}\overline{w'\theta'_v}\right]_{tur} + \left[\frac{g}{\overline{\theta}_v}\overline{w'\theta'_v}\right]_{cv} - \left[\frac{1}{\rho}\frac{\partial\overline{p'w'}}{\partial z}\right] - \left[\frac{\partial\overline{E'w'}}{\partial z}\right] - \varepsilon\end{aligned} \tag{46}$$

In (46) $\overline{E} = \frac{1}{2}\left(\overline{u'^2 + v'^2 + w'^2}\right)$ is the subgrid scale kinetic energy and ε is the dissipation of $\overline{E}$. Other symbols have their usual meaning. All terms on the r.h.s. represent the effect of physics. The first two terms are the horizontal sheer productions of turbulent kinetic energy. The third term involving vertical velocity variance has currently been neglected. Also the sixth term involving pressure correlations has been neglected.

The fourth term concerns the buoyancy generated subgrid scale kinetic energy from turbulence (index *tur*). Since the model also parameterizes cumulus clouds a corresponding term, the fifth term (index *cv*), is included to describe the subgrid scale kinetic energy generated from convective clouds. Currently an estimate of this term is made in the model's convection scheme (section 3.3). It is assumed that the production rate is proportional to the local buoyancy force associated with the convective clouds. The constant involved is set to $0.003\mathrm{m}\cdot\mathrm{s}^{-1}$.

The seventh term describes the vertical convergence of subgrid scale vertical transports of $\overline{E}$. Finally the last term is the dissipation term for $\overline{E}$, as mentioned above.

The parameterization of the turbulent transports relates the second order moments to mean variables by assuming relations of the form

$$-\overline{\zeta' w'} = K_\zeta\left(\frac{\partial\overline{\zeta}}{\partial z}\right); \quad \zeta = u, v, \theta, q, q_c, E. \tag{47}$$

In (47) K_ζ is an eddy exchange coefficient analogous to the molecular viscosity and diffusivity coefficients. The eddy exchange coefficients depend on $\overline{E}$:

$$K_\zeta = c_\zeta K_u \phi_3\left(Rs\right), \tag{48}$$

where c_ζ is a non-dimensional constant and $K_u = l\sqrt{\overline{E}}$ is the eddy exchange coefficient for momentum. ϕ_3 is a function of the dry Redelsperger number Rs

$$Rs = \frac{g}{\overline{\theta}_v}\frac{l^2}{\overline{E}}\left(1 + 0.61\,\overline{q}\frac{\partial\overline{\theta}}{\partial z} + 0.61\,\overline{\theta}\frac{\partial\overline{q}}{\partial z}\right). \tag{49}$$

ϕ_3 takes the form (Cuxart et al., 1995)

$$\phi_3 = (1 + 0.139 \cdot Rs)^{-1}, \tag{50}$$

where Rs is controlled by the condition $Rs = \max\{-3.924, \min\{Rs, 71935.252\}\}$. The scheme is prepared for a change from the "dry" variables θ, q and q_c to the "moist" variables θ_l (liquid water potential temperature) and $q_{tot} = q + q_c$ (total specific humidity). The Redelsperger number should for example be replaced by its moist version, i.e. the vertical gradients of $\overline{\theta}$ and $\overline{q}$ in (49) should be replaced by corresponding gradients of $\overline{\theta_l}$ and $\overline{q_t}$. Note that the covariance $\overline{E'w'}$ is retained in the equation (46). Accordingly, the list of variables in (47) is expanded with $\zeta = E$.

The dissipation ε is treated in by the following expression

$$\varepsilon = c_\varepsilon \cdot \frac{\overline{E}^{3/2}}{l}, \tag{51}$$

In the equation above l is a diagnostic mixing length. It is computed from

$$l = \sqrt{l_u \cdot l_d}, \tag{52}$$

where l_u and l_d are the distances an air parcel must be displaced upward or downward, respectively, before its $\overline{E}$ has been consumed by buoyancy. This formulation allows for diagnosing very large mixing lengths in neutra of unstable stratification. Currently the following constraint is imposed in order to avoid the potential risk of diagnosing excessive mixing near neutral atmospheric stratification.

$$l = \min\{l, l_{max1} + (l_{max2} - l_{max1}) \exp(-\frac{z^{'} - H_{pbl}}{H_{pbl}})\} \tag{53}$$

In (53) H_{pbl} is the boundary layer height (see section 6.3). $z^{'} = \max\{z, H_{pbl}\}$. Currently $l_{max1} = 100$ m, $l_{max2} = 500$ m. A diagnostic lower boundary condition is specified for $\overline{E}$ at the bottom level (index N). It is specified as

$$\overline{E}_N = 3.75u_*^2 + \delta_u \left[u_*^2 \left(-\frac{z_N}{L} \right)^{2/3} + 0.2w_*^2 \right], \tag{54}$$

with $\delta_u = 1$ or 0 if the surface layer is unstably or stably stratified, respectively. In the equation above L is the Monin-Obukov length scale (Businger et al., 1971). w_* is the convective velocity scale (Deardorff, 1972) and u_* is the friction velocity.

3.2.2. Numerical aspects

A semi-implicit treatment of the dissipation term of (46) has been made by writing (46) in the form

$$\frac{\partial \overline{E}}{\partial t} = F(\overline{E}, p_j), \quad j = 1, \ldots, J \tag{55}$$

In (55) p_j, $j \leq J$ are parameters other than $\overline{E}$. The virtues of time schemes involving the partial derivative with respect to the prognostic parameter considered, in this case $\overline{E}$, have been discussed in the literature, e.g., (Kalnay and Kanamitsu, 1988) and (McDonald, 1998). The solutions are normally stable and free of spurious oscillations (noise). This idea can in principle be implemented for all terms on the r.h.s. of (46). The scheme reads (evaluating F at the middle of the time step)

$$\frac{(\overline{E}_{n+1} - \overline{E}_n)}{\Delta t} = F_n + \frac{1}{2}\left(\frac{\partial F}{\partial \overline{E}}\right)_n (\overline{E}_{n+1} - \overline{E}_n) \tag{56}$$

Currently the idea expressed by (55) and (56) has been implemented for the dissipation term only (Sass, 1999).

The finite difference approximation to (56) and (55) is incorporated to the set of finite difference equations representing (46). The finite difference equation at model level k may be written

$$\begin{aligned}\overline{E}_{k,n+1} = \overline{E}_{k,n} + S_k + S_k^{\varepsilon} + S_k^{\varepsilon *} + A_{k,n}(\overline{E}_{k-1,n+1} - \overline{E}_{k,n+1}) \\ -C_{k,n}(\overline{E}_{k,n+1} - \overline{E}_{k+1,n+1}) - D_k^* \overline{E}_{k,n+1}\end{aligned} \tag{57}$$

In (57) S_k is a source term as a result of sheer production and buoyancy production of $\overline{E}$. The term S_k^{ε} is an explicit dissipation term in agreement with (51). The terms $S_k^{\varepsilon *}$ and D_k^* including $'*'$ are additional terms connected to the implicit treatment utilizing (55) and (56). $S_k^{\varepsilon *} = \frac{3}{4}\frac{c_\varepsilon}{L}\overline{E}_n^{\frac{3}{2}}\Delta t$ and $D_k^* = \frac{3}{4}\frac{c_\varepsilon}{L}\overline{E}_n^{\frac{1}{2}}\Delta t$.

When these terms are neglected, (57) reduces to the system using explicit dissipation. The coefficients $A_{k,n}$ and $C_{k,n}$ are coefficients involving eddy exchange coefficients describing turbulence effects from above and below level k, respectively.

From (57) one may isolate $\overline{E}_{k,n+1}$ on the left hand side giving

$$\overline{E}_{k,n+1} = \frac{\overline{E}_{k,n} + S_k + S_k^{\varepsilon} + S_k^{\varepsilon *} + A_{k,n}\overline{E}_{k-1,n+1} + C_{k,n}\overline{E}_{k+1,n+1}}{1 + A_{k,n} + C_{k,n} + D_k^*} \tag{58}$$

(58) describes a coupled set of equations in $\overline{E}_{k,n+1}$, $k = 2, \ldots, M-1$. M is the number of model layers. At the top ($k = 1$) an equation applies with $A_{1,n} = 0$. Similarly, for the bottom layer $C_{M,n} = 0$. The system of equations is solved by standard methods (successive elimination and backward substitution).

3.3. Convection and condensation

There has been many approaches during the past decades to describe the processes connected to clouds and condensation. This is related to the fact that a description of cloud and condensation processes involves both micro-physical aspects and a formulation of the vertical subgrid scale transports on all scales (turbulence and convection). Furthermore, it is often difficult to validate which formulations should be preferred by means of solid observational evidence. In recent years international comparisons have been useful

as a guidance, e.g., the GEWEX (Global Energy and Water Cycle Experiment) cloud system study (GCSS).

In the HIRLAM community a review has been written on the use of convection schemes in mesoscale models (Bister, 1998). One trend has been to apply mass flux concepts to parameterize convection. It may be argued that a mass flux approach is more physically based than are formulations relying on alternative approaches.

The different ideas and hypotheses behind parameterizing convection are reflected in the availability of different convection schemes for experimentation in the HIRLAM forecasting system. All schemes used in HIRLAM have 'cloud condensate' available as a prognostic variable which is advected by the model dynamics.

Currently the operational convection scheme is based on a moisture convergence closure and may be viewed as a further development of the ideas expressed by Kuo (1974). The scheme named STRACO stands for 'Soft TRAnsition COndensation' and concerns gradual transitions between convective and stratiform regimes.

The moisture convergence closure includes the effect of surface evaporation flux. A formulation of the vertical redistribution of cloud condensate is included which is an extension of the original formulations. Also convection can start from any level in the atmosphere whereas several convection schemes treat only deep convection originating from the lowest model layer.

The vertical extent of convection is determined by adiabatic cloud parcel lifting including latent heat release, starting with a small temperature excess as a 'trigger' for convection. Entrainment and detrainment are not explicitly taken into account during parcel lifting, but a simple constraint inhibits the vertical extent of convective clouds in case of a weak net convergence of moisture. The level of non-buoyancy determines the top of the convective layers. However, the effect of overshooting eddies penetrating into the stable layer above the moist unstable atmosphere is parameterized (Sass, 2001). Transports of heat and moisture, including cloud condensate, across an interface between a moist unstable and a stable atmosphere, is often termed 'shallow convection'. This effect is also parameterized when a deep moist convective atmosphere is involved.

Concerning the generation of subgrid scale kinetic energy due to convection (used in eq. 46) it is assumed that this effect can be estimated as a term proportional to the local buoyancy force.

Formally there is no limit on the possible number of convective entities in the vertical air column. The relevant equations are :

$$\left(\frac{\partial q}{\partial t}\right)_{ADC} = \left(\frac{\partial q}{\partial t}\right)_{AD}(1-\delta_*) + \widehat{Q}_a\beta\frac{F_q}{\widehat{F}_q}\delta_* + K_c q_c(q_s - q_e) + S_q + E_{pc} \qquad (59)$$

$$\left(\frac{\partial q_c}{\partial t}\right)_{ADC} = \left(\frac{\partial q_c}{\partial t}\right)_{AD} + \widehat{Q}_a(1-\beta)\frac{F_c}{\widehat{F}_c}\delta_* - K_c q_c(q_s - q_e) + S_c - G_{pc} \qquad (60)$$

$$\left(\frac{\partial T}{\partial t}\right)_{ADC} = \left(\frac{\partial T}{\partial t}\right)_{AD} + \frac{L'}{c_p}\left(\widehat{Q}_a(1-\beta)\frac{F_h}{\widehat{F}_h}\delta_* - K_c q_c(q_s - q_e)\right) + S_T - \frac{L'}{c_p}E_{pc} \qquad (61)$$

The left hand sides of these equations express the combined effect of both dynamical advection, turbulence and convection. $\frac{\partial}{\partial t}()_{AD}$ signifies a tendency excluding convection. $\widehat{Q}_a$ is the total moisture accession per unit mass and time in the convective cloud. L' and c_p represent the specific latent heat of fusion or sublimation, depending on the microphysical conditions, and the specific heat capacity at constant pressure, respectively.

F_h is a function describing the vertical variation of convective heating.

$$F_h = T_{vc} - T_{ve} + \epsilon_T \tag{62}$$

F_q is a function describing the vertical variation of convective moistening.

$$F_q = q_{sc} - q_e + \epsilon_q \tag{63}$$

F_c is a function describing the vertical variation of convective condensate supply.

$$F_c = q_{cc} + \epsilon_c \tag{64}$$

In the above equations for F_h, F_q and F_c index v stands for 'virtual'. Index e means 'environmental' (outside clouds). $\widehat{F}$ stands for a vertical average value for the convective cloud. Finally, c-index means a value applicable to cloud and s signifies a saturation value. The constants $\epsilon_T, \epsilon_q, \epsilon_c$ are currently set to zero.

The parameter β is a moistening parameter (Kuo, 1974). In the present scheme, contrary to models without prognostic cloud condensate, moistening can take place also from evaporation of cloud condensate.

$$\beta = \left(1 - \frac{\sum_{j=jbot}^{jtop} \frac{q}{q_s} \Delta p}{p_{jbot} - p_{jtop}}\right)^{\gamma_0} \tag{65}$$

Here p represents 'pressure', and $jbot$ and $jtop$ are the model level numbers for the bottom and top of convection, respectively. Currently γ_0 is set to a value of 2. The parameter δ_* is an important one, because it determines a link between convective moisture transports on one hand and turbulence plus dynamics effects on the other.

$$\delta_* = B \left(\frac{\Delta p_c}{p_{00}}\right)^{\gamma_1} \left(\frac{\Delta\theta}{\theta_{00}}\right)^{\gamma_2} \tag{66}$$

A resolution dependence has been introduced through the scaled latitude increment $\Delta\theta$ for the given resolution. The term involving Δp_c and p_{00} is a scaled cloud depth. Currently $\theta_{00} = 0.15°$ and $p_{00} = 10^4$ Pa. γ_1 and γ_2 are equal to 1. Both factors are constrained to be no larger than 1. The effect of this formulation is that δ_* goes to zero for extremely shallow phenomena and for very high horizontal resolution. A zero δ_* means that the convection scheme is decoupled as is reasonable in the limit of very shallow phenomena and high resolution where dynamics and turbulence should suffice. The factor B is a dimensionless buoyancy which is zero for a vanishing mean buoyancy in the convective cloud but becomes 1 when cloud buoyancy exceeds a small threshold. It serves to prevent an abrupt switch from stratiform to convective regime.

The third term in the main equations involving $(q_s - q_e)$ is an evaporation/sublimation term of cloud condensate. (K_c is a constant). A similar formulation, involving cloud cover as the leading term in place of q_c, has been used by others, e.g., (Tiedtke, 1993) in the ECMWF cloud scheme.

The fourth term in the same equations, involving S_q, S_c and S_T respectively, describes the effect of fluxes of heat and moisture across the interface between a moist convective atmosphere and the stable atmosphere above.

Finally, the terms involving G_{pc} and E_{pc} concern generation and evaporation of convective precipitation, respectively.

The equations above are applied in the layers of the convective entities while the stratiform condensation apply to the remaining parts of the atmosphere.

Associated with each convective and stratiform layer, respectively, is an equilibrium statistical distribution of total specific humidity around a grid box average value $\overline{q}_{tot}$.

In the stratiform case a symmetric rectangular density function is assumed and super-saturation is defined with respect to the grid box saturation specific humidity $q_s(\overline{T})$. In the convective case an asymmetric density function is assumed and super-saturation is defined with respect to a saturation humidity corresponding to a characteristic air parcel temperature T_c associated with convection. These assumptions make it feasible to define the fraction of the grid square which is saturated. This is by definition the grid box cloud cover.

The cloud fractions f_{cv} and f_{st} for convective and stratiform clouds respectively are given below

$$f_{cv} = \frac{1}{1 + \sqrt{\frac{q_s(T_c) - \overline{q}}{\overline{q}_c}}} \tag{67}$$

In (67) $q_s(T_c) \geq \overline{q}_{tot}$. An intermediate range is defined if $\overline{q}_{tot} \cdot (1 - A_{cv}) \leq q_s(T_c)$ and $q_s(T_c) < \overline{q}_{tot}$, where A_{cv} is a dimensionless threshold ~ 0.1 defining the width of the lower part of the probability density function of q_{tot}. For this intermediate range

$$f_{cv} = \frac{1}{2} + \frac{(\overline{q}_{tot} - q_s(T_c))}{2A_{cv}\overline{q}_{tot}} \tag{68}$$

Finally, f_{cv} is constrained to be equal to 1, if $q_s(T_c) < \overline{q}_{tot}(1 - A_{cv})$.

Correspondingly the following equation applies to the stratiform cloud cover f_{st}

$$f_{st} = \frac{1 + A_{st} - \frac{q_s(\overline{T})}{\overline{q}_{tot}}}{2A_{st}} \tag{69}$$

The formula above is only used in the range where it provides a cloud cover between zero and one. Outside this range the cloud cover is either 0 or 1, respectively. The probability function for q_{tot} also defines the equilibrium cloud condensate. It is assumed that also the specific humidity at sub-saturation is distributed equally as a rectangular probability function around the grid box average value $\overline{q}$. The amplitude of the fluctuating q_{tot}, as defined by A_{st} is constrained not to violate a rectangular distribution of q.

A similar approach for describing subgrid scale condensation has been used by others in the literature (Redelsperger and Sommeria, 1986). They emphasize the virtues of having a subgrid scale parameterization of condensation even at horizontal resolutions of a few kilometers grid distance.

The amplitude A_{st} of the symmetric density function for total specific humidity in the stratiform case should ideally not be constant with model resolution. The estimates (Redelsperger and Sommeria, 1986) that the subgrid scale effects should go to zero quite slowly at high resolution combined with typical values used in coarse resolution models have been used as a guidance for constructing (70) below. This effect of resolution is described by the first factor in (70). Formulations of A_{st} depending on other factors such as the height above ground have been suggested (Sundqvist et al., 1989). He assumes a decrease of A_{st} of the subgrid scale variability close to the ground. A similar idea has been adopted in the STRACO scheme as expressed by the term in the second brackets of (70).

$$A_{st} = A_{st1}\left(1 - \exp\left(-A_{st2}\sqrt{D_{gr}}\right)\right)\left(\frac{A_{st3} + A_{st4}(1-\sigma_{st}^3)}{A_{st3} + A_{st4}}\right) \tag{70}$$

In (70) $A_{st1} = 0.30$, $A_{st2} = 0.003$, $A_{st3} = 0.03$, $A_{st4} = 0.02$. $\sigma_{st} = \min(\frac{p}{p_{st}}, 1)$. $p_{st} =$ 1013 hPa. D_{gr} is the distance in metre between neighboring grid points.

A relaxation towards the equilibrium is applied to define stratiform condensation. However, the constraint is always imposed that gridbox saturation is not exceeded. Condensation associated with equilibrium is determined by a first order adjustment.

$$\Delta q_{st} = \frac{(q_c - q_{ceq})}{1 + f_{st}\frac{L}{c_p}\left(\frac{\partial q_s}{\partial T}\right)} \tag{71}$$

Due to the changing conditions as regards q, q_c and T in a model layer, the 'equilibrium' distribution is disturbed. This may, for example, happen with the onset of stratiform conditions after convection or vice-versa. To describe the actual transitions the cloud cover f is made time dependent by relaxing towards the equilibrium cloud cover f_{eq} which may be either a stratiform (f_{st}) or a convective equilibrium (f_{cv}).

$$\frac{\partial f}{\partial t} = -K_f(f - f_{eq}) \tag{72}$$

Currently $K_f^{-1} = 900$ s.

The micro-physics related to the condensation and precipitation processes follow rather closely the comprehensive treatment by (Sundqvist, 1993).

4. Surface treatment

4.1. Fluxes of momentum, heat and moisture at the surface

Turbulent surface fluxes in numerical weather prediction models are traditionally computed from drag formulae relating the surface fluxes to the mean states of the surface

and of the atmosphere at the observation height (in a numerical model, typically the lowest model level). The drag coefficient C_γ for a scalar variable γ is defined by the equation

$$\overline{w'\gamma'} = C_\gamma \Delta\gamma |\vec{V}_N| \tag{73}$$

in which $\overline{w'\gamma'}$ is the vertical turbulent kinematic flux of γ and $\Delta\gamma = \gamma_s - \gamma_N$.

The scalar variables and the wind vector on the right hand side of (73) are time averages like the flux term on the left hand side, but for convenience the averaging symbol has been omitted on the right hand side. The sign convention in (73) is such that upward fluxes are positive.

Over the ocean $\vec{V}_N$ should, strictly speaking, be measured in a frame moving with the ocean surface current and T_s should be the surface skin temperature.

The surface specific humidity q_s is not so obvious to specify as compared to surface wind speed $\vec{V}_s$ which may be assumed to be zero.

Over sea the saturation value $q_{sat}(T_s)$ with respect to the surface temperature is assumed. Over land a soil wetness parameter $F_{wet} = a_{w1} + (1 - a_{w1})(\frac{W_s}{W_{sat}})^{a_{w2}}$. W_s and W_{sat} are defined in the next subsection. $a_{w1} = 0.05$. $a_{w2} = 8$. The constraint is always imposed that the saturation value $q_{sat}(T_s)$ is never to be exceeded.

$$q_s = F_{wet} q_{sat}(T_s) + (1 - F_{wet}) q_N \tag{74}$$

In the current formulation

$$C_\gamma = C_{MN} \left(1 + \ln \frac{z_{0M}}{z_{0H}} \Big/ \ln \frac{z}{z_{0M}} \right)^{-1} \Psi_\gamma \left(Ri, \frac{z}{z_{0H}}, \frac{z}{z_{0M}} \right) \tag{75}$$

This formulation is used for different surface types and forecast scalar parameters. ($\gamma = M$ for momentum, correspondingly H and Q stand for heat and moisture transfer, respectively). The two factors in front of the function Ψ_γ form a neutral drag coefficient C_{γ_N}. For identical roughness lengths z_{0M} and $z_{0\gamma}$ the second factor in the brackets becomes unity and $C_{\gamma_N} = C_{MN}$.

$$C_{MN} = \left(\frac{k}{\ln(\frac{z}{z_{0M}})} \right)^2$$

$k \sim 0.4$ is the von Kármán constant.

The functions used for Ψ_γ follow the work of (Louis, 1979) and (Louis et al., 1982).

The following form applies to the unstable atmospheric boundary layer:

$$\Psi_\gamma = 1 + \frac{a_{\gamma U} Ri}{1 + b_{\gamma U} C_{\gamma_N} (Ri \frac{z}{z_{0M}})^{\frac{1}{2}}} \tag{76}$$

In (76) above Ri is the surface bulk Richardson number. $a_{mU} = 10$, $b_{mU} = 75$, $a_{HU} = a_{QU} = 15$ and $b_{HU} = b_{QU} = 75$.

A special situation occurs as the mean horizontal wind speed goes to zero in an unstable boundary layer. It turns out that realistic surface fluxes can be achieved in the

framework of the existing formula provided that z_{0M} in (76) is replaced by the length scale d_γ, (Nielsen, 1999), where $d_M = 1.03\frac{\nu}{u_{fc}}$, $d_H = d_Q = 1.14\frac{\nu}{u_{fc}}$, and ν is a kinematic viscosity of air. u_{fc} is a velocity scale associated with free convection

$$u_{fc} = \left(\frac{g}{\theta_v}\Delta\theta_v\nu\right)^{\frac{1}{3}} \tag{77}$$

In (77) g is the acceleration of gravity and $\Delta\theta_v$ expresses the virtual potential temperature difference between the atmosphere and the sea surface.

For the stable boundary layer the corresponding formula is

$$\Psi_M = \frac{1}{1 + \frac{a_{MS}Ri}{\sqrt{1+b_{MS}\,Ri}}} \tag{78}$$

In (78) above $a_{MS} = 10$, $b_{MS} = 1$.

For heat and moisture the following function is used

$$\Psi_\gamma = \frac{1}{1 + a_{\gamma S}Ri\sqrt{1 + b_{\gamma S}Ri}} \tag{79}$$

$a_{HS} = a_{QS} = 10$ and $b_{HS} = b_{QS} = 1$.

For flux computations over land and sea ice the potential of the formulae above to incorporate effects of separate roughness lengths for momentum, heat and moisture, is not used. Currently the roughness lengths for heat, moisture and momentum are taken to be equal. The actual value of roughness depends strongly on land surface type according to basic theories of the planetary boundary layer (Garrat, 1977). The actual values are computed in the climate field generation (see subsection 4.3). Values of heat and moisture roughness up to 0.5 m are allowed for. However, it turns out that larger values for momentum roughness are needed to describe surface drag in a formulation based on roughness length. This is because the effect of subgrid scale orography is significant. The current algorithm for such computations makes the momentum roughness proportional to the variance of subgrid scale orography. In this way it turns out that momentum roughness over land can achieve values of several metre. The roughness length for ice is taken to be 0.03 m which is substantially higher than current estimates for a plane ice surface, in order to account for horizontal irregular features occurring in natural ice fields.

To complete the parameterization for surface flux computations over sea the ratio of the roughness lengths z_{0M}/z_{0H} and z_{0M}/z_{0Q} must be related to known quantities. Measurements over sea indicate that the surface roughness lengths for momentum, sensible heat and moisture are different, (DeCosmo et al., 1996). The main reason is probably that form drag (i.e., momentum transport by pressure forces) in the presence of sea waves enhances the momentum transfer, while the heat and moisture transfers at the air-sea interface are controlled by molecular diffusion alone.

According to observations and laboratory experiments z_{0M} depends on the sea state. At low wind speeds laboratory experiments indicate that the sea surface becomes aerodynamically smooth with z_{0M}=$0.11\,\nu/u_*$. At sufficiently high wind speeds the sea surface becomes aerodynamically rough. In the latter conditions the Charnock formula

$z_{0M} = \beta u_*^2/g$, (Charnock, 1955) with a value of β in the range of 0.011 to 0.032, are widely used. In numerical models values of β in the interval of 0.014 to 0.0185 are recommended (Garrat, 1992). We introduce a transition in z_{0M} from a smooth to a rough sea surface depending on wind speed $|\vec{V}_N|$, where index N refers to the height of the lowest model level. The interpolation formula for z_{0M} is specified as

$$z_{0M} = (1 - \xi(\mathrm{u}))\, 0.11\, \nu/u_* + \xi(\mathrm{u})\beta \frac{u_*^2}{g}\,, \tag{80}$$

with

$$\xi(\mathrm{u}) = \left[\max\left(\min\left(\frac{u - u_s}{u_r - u_s}, 1\right), 0\right)\right]^{1/2}\,. \tag{81}$$

In (80) and (81) $u = |\vec{V}_N|$, $u_s = 3.0$ m/s and $u_r = 5.0$ m/s. According to (80) and (81) the sea surface is considered to be smooth for $u \leq 3$ m/s and rough for $u \geq 5$ m/s. The transition interval is somewhat smaller than the interval from 2.5 to 5.5 m/s usually found in the literature e.g., (Garrat, 1992). Over open sea (here defined as fraction of sea equal to 1) β has been set to 0.014, otherwise $\beta = 0.032$. The former value fits measurements over the open ocean quite well e.g., (Yelland and Taylor, 1996; Grachev et al., 1998). A higher value of β (larger momentum flux) in shallow coastal waters is supported by measurements (Oost, 1998; Hansen and Larsen, 1997; Maat et al., 1991), although the governing parameter for z_{0M} seems to be the wave age.

We assume that z_{0H} and z_{0Q} can be related to z_{0M}. Observational evidence of a relation between z_{0M} and z_{0Q} has been presented for example by DeCosmo *et al.*, 1996. Dependence of z_{0H} and z_{0Q} on z_{0M} are also key features in 'surface flux over sea' models by e.g. (Clayson et al., 1996; Liu et al., 1979; Brutsaert, 1975). In our parameterization z_{0H} and z_{0Q} are related to z_{0M} by formulae suggested in Garratt, 1992. In terms of the roughness Reynolds number, Re_*, the relations take the form

$$\ln \frac{z_{0M}}{z_{0H}} = \alpha_H Re_*^{1/4} - 2\,, \tag{82}$$

$$\ln \frac{z_{0M}}{z_{0Q}} = \ln \frac{z_{0M}}{z_{0H}} - \alpha_Q Re_*^{1/4}\,, \tag{83}$$

in which Re_* is defined as

$$Re_* = \frac{z_{0M} u_*}{\nu}\,, \tag{84}$$

i.e., by the sea surface momentum roughness length (z_{0M}), the surface friction velocity (u_*) and the molecular kinematic viscosity coefficient for air ($\nu \simeq 1.5 \cdot 10^{-5}\,\mathrm{m}^2/\mathrm{s}$). Over a rough sea α_H=2.48 and α_Q=0.2. With the transition from a smooth to a rough sea surface given by (81), and over a smooth surface with the requirement $z_{0\gamma} \cdot u_*/\nu = S_\gamma$ for $\gamma = H, Q$ and $S_H \approx 0.2$ and $S_Q \approx 0.3$ (Garrat, 1992), the coefficients α_H and α_Q in (82) and (83) become

$$\alpha_H = 0.05\xi(\mathrm{u}) + 2.43\,, \tag{85}$$

$$\alpha_Q = -0.50\xi(\mathrm{u}) + 0.70\,. \tag{86}$$

4.2. Surface energy and moisture budget

In the previous section the relevant interactions between atmosphere and surface were described, except as regards radiation fluxes which need also to be considered to describe the atmospheric forcing of the surface. The present treatment of the surface consists of separate computations for sea or lake surface on the one hand, and a land surface possibly including ice on the other. In the former case the interactions with the atmosphere happens via the fluxes of momentum, heat and moisture as described above, and as a result of radiation. In the infrared part of the spectrum the radiation is exchanged almost as black body radiation corresponding to the sea surface temperature (SST). The emissivity of the surface is currently taken to 0.95. The SSTs are achieved from the daily values received from ECMWF. An interpolation procedure takes into account the distribution of sea and land. Any net energy loss from the sea surface has no direct consequences for the model SST because this parameter is not a prognostic variable, but is locally fixed in time during a forecast. The fraction of ice in a grid square is determined from an analysed field received daily from the ECMWF forecast model.

The energy and moisture budget of a land surface needs to be treated in a prognostic sense since the forecasting of diurnal variations of meteorological parameters close to the ground is vital. The present surface treatment over land is simple. There are two prognostic surface temperatures, namely T_s and T_d respectively. T_s represents a surface temperature, and T_d a temperature at an intermediate level above a climatic deep soil temperature. Similarly, two prognostic equations are included for soil moisture (W_s and W_d). These variables represent soil moisture at the upper and at the intermediate level, respectively. Currently there is no assimilation scheme for soil parameters such as temperature and moisture. Instead the initial values used in a forecast come from a short range forecast.

4.2.1. Equations for soil variables

The evolution of temperature and soil water is assumed to obey a simple diffusion equation in a simple two layer soil model. Also an equation for snow depth Sn is available. The five prognostic equations are given below.

$$\frac{\partial T_s}{\partial t} = \frac{1}{\rho_s c_s D_1} \sum_i \Phi_i + \frac{\kappa_0 (1 - k_{sn} F_{sn})(T_d - T_s)}{0.5 D_1 (D_1 + D_2)} \tag{87}$$

In the equation above $\sum_i \Phi_i = \Phi_R + \Phi_H + \Phi_Q$ are the surface net fluxes due to radiation, sensible heat and latent heat, respectively. $F_{sn} = \min(\frac{H_{sn}}{H_{snc}}, 1)$ is a snow fraction, with H_{sn} being snow depth and $H_{snc} = 0.015$ m a threshold snow depth in an equivalent height of water. T_s (K) is the soil temperature in the upper soil layer. T_d is the soil temperature in the intermediate soil layer. ρ_s is the soil density (kg/m^3), c_s is the specific heat capacity of the soil $\left(\frac{\text{J}}{\text{kg K}}\right)$, κ_0 is the heat diffusivity of soil without snow cover (m^2/s). k_{sn} is a dimensionless constant used to reduce heat diffusivity if snow cover is positive.

Currently, $\rho_s c_s = 2.7{\cdot}10^6\,\mathrm{J/(m^3\,K)}$, $k_{sn} = \frac{2}{3}$, $D_1 = 0.07$ m, and $D_2 = 6D_1$.

$$\frac{\partial T_d}{\partial t} = -\frac{\kappa_0(T_d - T_s)}{0.5D_2(D_1 + D_2)} + \frac{\kappa_0(T_{cli} - T_d)}{D_2 D_3} \tag{88}$$

T_{cli} is a climatic deep soil temperature updated every month. $D_2 = D_3 = 6D_1$ (m).

Similarly, the equations for soil water are

$$\frac{\partial W_s}{\partial t} = (1 - F_{sn})\Phi_Q + P_{rn} + M_{sn} + \frac{\lambda(W_d - W_s)}{0.5D_1(D_1 + D_2)} \tag{89}$$

W_s is the soil water in the top layer (m). W_d is soil water in the second soil layer times $\frac{D_1}{D_2}$ (m). This means that it is scaled to the depth of the top layer. P_{rn} is the rain flux density reaching the ground ($\frac{\mathrm{kg}}{\mathrm{m^2\,s}}$). M_{sn} is the change in snow depth per unit time. λ is a diffusivity for conduction of soil water. $\lambda = 1.0{\cdot}10^{-7}\,\mathrm{m^2/s}$.

$$\frac{\partial W_d}{\partial t} = -\frac{\lambda(W_d - W_s)}{0.5D_2(D_1 + D_2)} + \frac{\lambda(W_{cli} - W_d)}{D_2 D_3} \tag{90}$$

Snow depth H_{sn} is updated if the the physiographic data-fields 'fraction of land' or 'fraction of ice' is positive in a model grid square.

$$\frac{\partial H_{sn}}{\partial t} = F_{sn}\frac{\Phi_Q}{\rho_{\mathrm{H_2O}}} + P_{sn} - M_{sn} \tag{91}$$

$\rho_{\mathrm{H_2O}}$ is the density of water ($\mathrm{kg/m^3}$).

The treatment of 'runoff' is very simple since instantaneous runoff of soil water is assumed if soil water exceeds 0.02 m (upper layer). This corresponds approximately to a volumetric water amount of 0.29.

Snow melt is crudely accounted for, being proportional to mean excess of land temperature over the melting point. The mean surface temperature, T_s, is allowed to rise above the melting point before all snow has melted, in order to account for subgrid scale temperature variation.

4.2.2. Numerical aspects

In order to prevent numerical instability, the equations above for the soil parameters γ are solved by the following semi-implicit method:

$$\frac{\partial \gamma}{\partial t} = \Psi(\gamma) \tag{92}$$

In the equation above Ψ is linearized in the following way: (n is the current time step, $n + 1$ is the new time step)

$$\Psi(n+1) = \Psi(n) + \frac{1}{2}\frac{\partial \Psi}{\partial \gamma}(\gamma(n+1) - \gamma(n)) \tag{93}$$

As a consequence of the equations above, the partial derivatives of surface fluxes with respect to the surface variable γ need to be computed.

4.3. Physiographic data

An accurate specification of the lower boundary conditions associated with atmospheric forecasts is very important, especially due to the need to forecast weather parameters close to the ground. Various surface fields (e.g., surface geopotential, surface albedo, surface roughness, soil temperature and soil moisture, and fractions of a grid square with sea (lake), ice and different types of land) are needed to carry out adequate surface computations. High quality and high resolution physiographic data are needed as a basic source to compute the fields accurately. New databases and new software have been introduced recently for this generation of surface fields. The new software makes use of the *Hierarchical Data Format* HDF, which makes it possible to unify the format of the input files for the computation of the needed surface fields for HIRLAM.

The data bases are of different origin. One set used is the *Global 30 Arc Second Elevation data* (GTOPO30). A second one is the *Global Land Cover Characteristics data* (GLCC). These data sources have a horizontal resolution of about 1 km. Improved accuracy on the land use over Denmark has been obtained with local data from "Kort og Matrikelstyrelsen" in Copenhagen. The processing of data for generation of physiographic data for HIRLAM has been documented (Sattler, 1999).

5. Data assimilation

Application of a data assimilation system is necessary in order to analyse the initial state of a given forecast. Normally, the spatial density of observations is much smaller than the number of grid points in a forecast model. As a consequence, it is a challenge to correct the model in an optimal way from the model's 'first guess'. Observation density, however, varies a lot, depending on the type of observations considered. In recent years various types of satellite data provide a huge source of data which is potentially of great value for the meteorological forecast models.

Advanced data assimilation systems have been developed, with a view to incorporate new data types in the analysis procedure. The name 3D-Var is assigned to variational methods involving analyses at a given time utilizing information from the 3 spatial dimensions. Similarly 4D-Var includes the spatial dimensions plus data from several time levels in the assimilation procedure.

In the HIRLAM community a 3D-Var system has been developed (Gustafsson et al., 2001; Lindskog et al., 2001; Undén et al., 2002). This system is used operationally at DMI (See Appendix A). A documentation of experimental results obtained prior to the first operational implementation of 3D-Var at DMI is available (Mogensen et al., 2000).

5.1. Minimization in 3D-Var

The theory of variational data assimilation involves the minimization of a 'cost-function' J which is a sum of two parts J_b and J_o.

$$J = J_b + J_o = \frac{1}{2}(\mathbf{x} - \mathbf{x^b})^T \mathbf{B^{-1}} (\mathbf{x} - \mathbf{x^b}) + \frac{1}{2}(H\mathbf{x} - \mathbf{y})^T \mathbf{R^{-1}} (H\mathbf{x} - \mathbf{y}). \qquad (94)$$

In (94) $\mathbf{x}$ is a model state during iteration, $\mathbf{x^b}$ is the model 'first guess' (background) model state, obtained as a short range forecast from a previous analysis. $\mathbf{y}$ refers to a vector with all observations. H is the so called 'obs-operator' which produces a model counterpart of an observation, that is, a quantity valid at the observed location is created by this operator, acting on the model state. The matrix $\mathbf{B}$ describes the background model's error covariances while $\mathbf{R}$ is a matrix containing the observation error covariances.

In the HIRLAM formulation an incrementatal approach is used (Gustafsson et al., 2001) where the following transformed control variables are used:

$$\delta\mathbf{x} = \mathbf{G}\left(\mathbf{x} - \mathbf{x^b}\right) \tag{95}$$

where $\mathbf{G}$ is an operator which (optionally) truncates the resolution of the analysis increment to a lower resolution. In addition the observation operators are linearized around the background state. With these modifications the cost functions is reformulated as

$$J = J_B + J_o = \frac{1}{2}\delta\mathbf{x}^T\mathbf{B}^{-1}\delta\mathbf{x} + \frac{1}{2}\left(H\mathbf{x^b} + \mathbf{H}\delta\mathbf{x}^T - \mathbf{y}\right)^T\mathbf{R}^{-1}\left(H\mathbf{x^b} + \mathbf{H}\delta\mathbf{x}^T - \mathbf{y}\right) \tag{96}$$

where $\mathbf{H}$ is the linearized observation operator of the full observation operator (H). With this formulation the minimization results in an analysis increment of lower resolution than the background field. The full resolution analysis is constructed by transforming the analysis increment to full resolution and adding it to the background field.

To carry out the minimization of the cost-function (94) is a demanding iterative task. Regarding practical applications it turns out that the minimization procedure requires a 'preconditioning' in order to limit the amount of iterations. The scheme used involves a complex transformation between model state and spectral space. This transformation takes into account horizontal and vertical error correlations. In addition, the wind error is transformed to an ageostrophic wind error, assuming that the wind error field is in near geostrophic balance. Hence the geostrophic wind error determined from the error in the mass field is subtracted from the wind error.

It is noted that the model state $\mathbf{x}$ entering the minimization is currently lacking some model variables which are a part of the total model state, e.g., the surface variables. Also the three-dimensional model parameters q_c (cloud condensate) and E (sub-grid scale kinetic energy) are left out for the time being due to lack of observations. Hence the task of the minimization is to find an increment $\delta\mathbf{x}$ defined below

$$\delta\mathbf{x} = \begin{pmatrix} \delta\mathbf{u} \\ \delta\mathbf{v} \\ \delta\mathbf{T} \\ \delta\mathbf{q} \\ \delta\ln\mathbf{p_s} \end{pmatrix}$$

$\mathbf{u}$ and $\mathbf{v}$ are the horizontal wind component vectors. $\mathbf{T}$ and $\mathbf{q}$ are the temperature and specific humidity vectors, and $\ln\mathbf{p_s}$ describes the logarithm of surface pressure. The minimization computation is carried out in spectral space.

The estimation of background error statistics makes use of accumulated differences between +24 hour and +48 hour forecasts that are valid at the same time. These statistics of forecast differences are considered as an approximation to the true forecast errors in the so called 'NMC method' (Parrish and Derber, 1992; Rabier et al., 1998). Standard deviations of the forecast differences are rescaled to match the amplitude of +3 hour forecast errors. An empirical scaling factor of 0.6 is used (Berre, 2000). Assumptions of horizontal homogeneity and isotropy are currently imposed for the structure functions. The treatment of observations is described below.

5.2. The observation handling system

Observations in BUFR format are input to a program (OBSPROC) which produces a file in the 'Central Memory Array' (CMA) format. While the CMA file is being prepared, necessary information is checked for and, if necessary, observed values are transformed into those used directly by the variational data assimilation. The specified observation error standard deviations are assigned (Lindskog et al., 2001; Undén et al., 2002). The CMA file is input to HIRVDA (HIRlam Variational Data Assimilation). The HIRVDA observation screening performs quality control using various algorithms, including a comparison with the model background field, data rejection and data thinning to select only those observed values that actually will be used by the variational data assimilation. The HIRLAM 3D-Var produces the analysis file, and the CMA file is updated with the appropriate monitoring information, such as quality control flags and observation minus analysis departures. The feed-back statistics are produced from the updated CMA files for diagnostic purposes.

The screening decisions are summarized below:

- Logical checks: It is verified that observations are situated within the analysis area and that SHIP (DRIBU) reports originate from ocean areas.
- Representativity checks: For example, stations situated too far away from model orography are rejected.
- Background quality control: The background model state is projected on a given observation y_i to be checked, using the obs-operator H. The squared background departure from the observed value is calculated and normalized with the sum of the observation error variance $\sigma_{o,i}^2$ plus the background error variance $\sigma_{b,i}^2$. The result L of this normalization is only allowed to be within a specified interval $L_1 \leq L \leq L_2$.

  $$L = ([H(\mathbf{x}^b)]_i - y_i) \cdot |([H(\mathbf{x}^\mathbf{b})]_i - y_i)|/(\sigma_{b,i}^2 + \sigma_{o,i}^2)$$

  The values of L_1 and L_2 depend on the type of observation and may be regarded as tuning constants. The σ_b -values vary spatially representing differences in flow characteristics in different geographical areas, as well as from variation in station density. The external file of σ_b-values is based on ECMWF forecasts and provides a global coverage, allowing the data-assimilation system to be run over different areas.

- Multilevel check of multilevel report data: If more than four consecutive levels are flagged suspicious, all of these data are rejected.

- Station level: For land surface stations the observed station altitude pressure and the corresponding geopotential height are selected rather than the mean sea level pressure and the corresponding zero height.

- Data redundancy check: All collocated land surface observations which have passed the former tests are then considered. Only the observation closest to the time of analysis is accepted. Radiosondes and PILOT ballon reports are simultaneously checked. If both types of reports exist from the same station the radiosonde report is selected by preference. Furthermore, in the case of multiple reports of the same type, the one closest to analysis time is chosen.

- Moving platform check: A thinning is applied by retaining only the observations closest to the time of analysis from the same station identifier. The minimum horizontal distance allowed between two moving platform observation reports of the same type has initially been set to half a grid distance. In addition, for aircraft observations, a thinning is applied in the vertical by allowing a minimum vertical pressure difference of 50 hPa.

- A variational quality control has been formulated and implemented. The variational quality control (Lorenc, 1986; Lorenc and Hammon, 1988; Andersson and Järvinen, 1999) incorporates the concept of probability of 'gross errors' and 'random errors'. The impact of a single observation to the observational part of the cost-function may be computed, with and without variational quality control, respectively. The relative magnitude of these two terms determines if the observations is rejected in the variational quality control.

Currently, the following observations are used: SYNOP (pressure), SHIP (pressure), DRIBU (pressure), PILOT (wind at all significant levels), TEMP (temperature, wind and humidity at all significant levels), AIREP and AMDAR/ACARS (wind, temperature).

After an analysis has been made the model balance has been affected to some extent. As a consequence, an initialization scheme is used prior to the start of the model forecast. The normal mode initialization (Källén, 1996) removes partly the gravity waves caused by the model imbalance after the analysis.

6. Diagnostic output

A number of special output parameters are produced in connection with the HIRLAM forecasts. These are closely related to some of the main forecast variables. The formulae associated with some key diagnostic parameters are given below.

6.1. Wind at 10 metre

The formulae used are derived by a vertical integration of basic formulae from boundary layer theory (Paulson, 1970; Businger et al., 1971). It is assumed that the diagnosed winds apply to a level between the surface and the height of the lowest model layer. For the unstable boundary layer we get for the wind component u in the west-east direction

$$\begin{aligned} u_{(Z)} &= u_{(N)} - \frac{u_*}{k}\left(-\ln\left(\frac{Z}{Z_N}\frac{(1+X_N^2)}{(1+X^2)}\right) - \right. \\ &\left. 2\ln\left(\frac{1+X_N}{1+X}\right) + 2\left(\tan^{-1}(X_N) - \tan^{-1}(X)\right) + b_{m1}u_*\right) \qquad (97) \\ X &= \left(1-15\frac{Z}{L}\right)^{\frac{1}{4}}, \quad X_N = \left(1-15\frac{Z_N}{L}\right)^{\frac{1}{4}} \end{aligned}$$

k is the von Kármán constant, L is the Monin-Obukov length scale, u_* is the friction velocity. $b_{m1} = 1.0$ A similar formula applies to the wind component v in the northerly direction.

For the stable planetary boundary layer the following modified form of the integrated profiles is used in order to guarantee that the diagnosed wind speed is no larger than that provided by the lowest model layer wind.

$$u_{(Z)} = \frac{u_*}{k}\ln\left(\frac{Z}{Z_0}\right) + u_N\left[1-\exp\left(-\frac{b_{m2}}{k}\frac{u_*}{u_N}\frac{Z}{L}\right) + b_{m1}u_*\right] \qquad (98)$$

$b_{m2} = 4.0$. A similar equation applies to $v_{(Z)}$. The term involving b_{m1} (not present in the work of Paulson (1970) and Businger et al. (1971)) is included to obtain a better fit of the diagnosed wind to the observations.

6.2. Temperature and humidity at 2 metre

The equations for temperature and specific humidity are given below applying similar principles as mentioned above for the wind components (θ_* and q_* are the corresponding surface fluctuations for temperature and specific humidity, respectively). For the unstable boundary layer we get for the potential temperature (θ) and specific humidity (q):

$$\theta_{(Z)} = \theta_{(N)} - \frac{\theta_*}{k}\ln\left(\frac{Z_N}{Z}\frac{(1+Y)^2}{(1+Y_N)^2}\right) \qquad (99)$$

$$q_{(Z)} = q_{(N)} - \frac{q_*}{k}\ln\left(\frac{Z_N}{Z}\frac{(1+Y)^2}{(1+Y_N)^2}\right) \qquad (100)$$

$$Y = \sqrt{1-9\frac{Z}{L}}, \quad Y_N = \sqrt{1-9\frac{Z_N}{L}}$$

For the stable planetary boundary layer the corresponding equations are

$$\theta_{(Z)} = \theta_s + \frac{\theta_*}{k}\ln\left(\frac{Z}{Z_0}\right) + \Delta\theta_N\left[1-\exp\left(-\frac{b_h}{k}\frac{\theta_*}{\theta_N}\frac{Z}{L}\right)\right] \qquad (101)$$

$$q_{(Z)} = q_s + \frac{q_*}{k}\ln\left(\frac{Z}{Z_0}\right) + \Delta q_N\left[1 - \exp\left(-\frac{b_q}{k}\frac{|q_*|}{q_N}\frac{Z}{L}\right)\right] \tag{102}$$

Currently $b_h = b_q = b_{m2}$, $\Delta\theta_N = \theta_N - \theta_s$, $\Delta q_N = q_N - q_s$.

6.3. Boundary layer height

A boundary layer height H_{pbl} which is useful for applications related to air pollution is computed diagnostically as an output field from parameters produced during the forecast

$$Ri_b = \frac{\frac{g}{\theta_{vs}}(\theta_{vh} - \theta_{vs})(z_h - z_s)}{(u_h - u_s)^2 + (v_h - v_s)^2 + bu_*^2} \tag{103}$$

This equation (Vogelezang and Holtslag, 1996) is solved iteratively using a criterion that the bulk Richardson number Ri_b must not exceed a critical value. Subscripts 's' and 'h' denote the top of the surface layer ($z_s = 0.1\,h$) and the top of the boundary layer, respectively. Guided by sensitivity experiments Ri_b is set to 0.25 and $b = 100$. $H_{pbl} = z_h$ when the critical value of the Richardson number is reached.

6.4. MSLP

Charts of mean sea level pressure (MSLP) are widely used in weather forecasting. An obvious problem exists in the case of high elevated ground. Traditionally a fictitious MSLP is estimated using near surface information on temperature and assumptions on a temperature lapse rate 'below ground' to estimate a reasonable MSLP as an extrapolation. This method, however, is quite sensitive to the assumptions made, in particular in the case of very high mountains. To minimize these problems, the vertical extrapolation is replaced by investigating a horizontal variation. This method has been described in the literature (Pielke and Cram, 1987).

The diagnosed values P_{msl} of a non-divergent surface MSLP, is obtained from a Poisson equation

$$\frac{\partial^2 P_{msl}}{\partial x^2} + \frac{\partial^2 P_{msl}}{\partial y^2} = \frac{\partial}{\partial x}\left(\frac{(v_g f)}{\theta}\right) - \frac{\partial}{\partial y}\left(\frac{(u_g f)}{\theta}\right) \tag{104}$$

In the equation above u_g and v_g are geostrophic wind components and f is the Coriolis parameter. The relationship has been derived by taking the curl of the expressions below for the surface geostrophic winds.

$$v_g = \frac{\theta}{f}\frac{\partial \tilde{P}_s}{\partial x} + \frac{g}{f}\frac{\partial z_g}{\partial x} = \frac{\theta}{f}\frac{\partial P_{msl}}{\partial x} \tag{105}$$

$$u_g = -\frac{\theta}{f}\frac{\partial \tilde{P}_s}{\partial y} - \frac{g}{f}\frac{\partial z_g}{\partial y} = -\frac{\theta}{f}\frac{\partial P_{msl}}{\partial y} \tag{106}$$

In the expressions above z_g is the height of the ground above mean sea level, and

$$\tilde{P}_s = c_p\left(\frac{p}{p_0}\right)^{\frac{R}{c_p}}, \quad p_0 = 1000 \text{ hPa}.$$

In order to solve the Poisson equation (104) it is necessary to compute the potential temperature θ. Also the lateral boundary values of P_{msl} are needed. These are supplied by a traditional extrapolation procedure. Otherwise a solution of the Poisson equation is sufficient to derive the diagnosed (non-divergent) MSLP in the internal model area. The solution is found by a traditional relaxation method.

6.5. Diagnostic cloud cover

The 3-dimensional (volumetric) cloud cover field computed during the model run needs to be processed further in order to be comparable to synoptic observations of clouds. Normally, assumptions about cloud overlap in the vertical have to be made in order to provide a model estimate of total cloud cover. Currently a combination of *maximum* and *random* cloud overlap in the vertical is used in the post-processed cloud cover f_{tot}

$$f_{tot} = 1 - (1 - f_H) \cdot (1 - f_M) \cdot (1 - f_L) \tag{107}$$

In (107) f_{tot} is the cloud cover to be compared with synoptic observations of total cloud cover. f_H, f_M and f_L are the fractional cloud cover of high clouds, medium level clouds and low level clouds, respectively. These are individually computed as the maximum value of the fractional cloud covers in relevant parts of the atmosphere. The fraction of the atmosphere used to define high level clouds is the top 10-40 percent of the atmospheric mass. The presence of clouds at even higher levels are discarded. The corresponding assessment of medium level clouds is made from the atmospheric layers located between 40 and 80 percent of the atmospheric mass counted from above. The additional lower cloud levels, excluding the lowest atmospheric model level, is used to assess the low level cloud cover. A possible fractional cloudiness in the lowest model layer is assigned as *fog*.

6.6. Visibility

An empirical diagnostic measure of visibility in *metres* has been developed, based on a statistical investigation of synoptic observations of visibility in Denmark. The following equation (Kunkel, 1984) has been utilized

$$VIS_{2m} = dC_*^{-0.88} \tag{108}$$

In (108) VIS_{2m} is the horizontal visibility estimated at a height of 2 m. C_* is an effective (fictitious) volumetric cloud water amount and d is a constant. The statistical investigation and the derivation of the diagnostic formulae is available, (Petersen and Nielsen, 2000). In (108) C_* is described as a sum of three terms according to

$$C_* = \sigma_{bg} + \sigma_{as} + \sigma_t \tag{109}$$

The first term σ_{bg} represents the effect of a *background* (average) aerosol content while the second term σ_{as} describes the statistical effect of wind speed and direction on aerosol characteristics. Finally, the third term is a complex expression taking into account several effects such as the dew point depression at a height of 2 metres, the wind speed, the precipitation intensities of rain and snow, the cloud cover and the solar zenith angle. The detailed documentation (Petersen and Nielsen, 2000) also contains a verification of the diagnostic formula showing generally good agreement with observed visibility in Denmark.

6.7. Wind gusts

A diagnostic formula describing wind gusts in the surface layer has been developed, based on similarity theory (Nielsen and Petersen, 2001). The following formula is used for the gust factor, that is, the ratio $\frac{G_u}{U}$ between wind gust and mean wind at the anemometer level:

$$\frac{G_u}{U} = 1 + j_u \cdot \left(c_b \frac{w_*}{U} + c_n \frac{u_{*0}}{U} \right) + j_s c_n \frac{u_{*0}}{U} \tag{110}$$

In (110) G_u is the wind gust at the diagnostic level with mean wind speed U. The factors j_u and j_s are integers with values 0 or 1. $j_u = 1$ for an unstable planetary boundary layer and is 0 in the stable case. $j_s = 1 - j_u$. The velocity w_* is the convective velocity scale (Deardorff, 1972), and u_{*0} is the surface friction velocity. The values of the constants c_b and c_n are dependent on how the wind gust is defined. The values increase if the time averaging period for the wind gust is shortened (Krayer and Marshall, 1992).

6.8. Icing index for aircraft

An index $ICEIN$ has been implemented to assess the risk of, and the intensity of icing up of aircraft. This index originates from the Swedish Defence administration, (Olofsson et al., 1999). The index can be calculated and displayed for any given pressure level. If the specific cloud water q_c (kg water)/(kg air) is greater than 0 and the temperature is below the freezing point index A is calculated as follows:

$$A = 5.0 + \ln(1000 \cdot q_c) \tag{111}$$

In (111) A is a number normally between 0 and 5. The final index $ICEIN$ is then calculated as a function of the vertical velocity w in $\frac{\text{cm}}{\text{s}}$:

$$ICEIN = \begin{cases} A - 1 & \text{if } w \leq 0 \\ A & \text{if } w > 0 \text{ and } w \leq 5.0 \\ A + 1 & \text{if } w > 5.0 \text{ and } w \leq 10.0 \\ A + 2 & \text{if } w > 10.0 \text{ and } w \leq 15.0 \\ A + 3 & \text{if } w > 15.0 \text{ and } w \leq 20.0 \\ A + 4 & \text{if } w > 20.0 \end{cases}$$

The maximum value of $ICEIN$ is by definition 9. The risk of icing up is described as a gradually increasing risk as the $ICEIN$ index increases from zero (no risk) to 9 (great risk)

Appendix A. DMI model setup (April 2002)

The operational system consists of four nested models named DMI-HIRLAM-G, DMI-HIRLAM-N, DMI-HIRLAM-E and DMI-HIRLAM-D, respectively. In short, the models are abbreviated 'G', 'N', 'E', and 'D', respectively. The model integration areas are shown in the figure below. The lateral boundary values of model 'G' are provided by

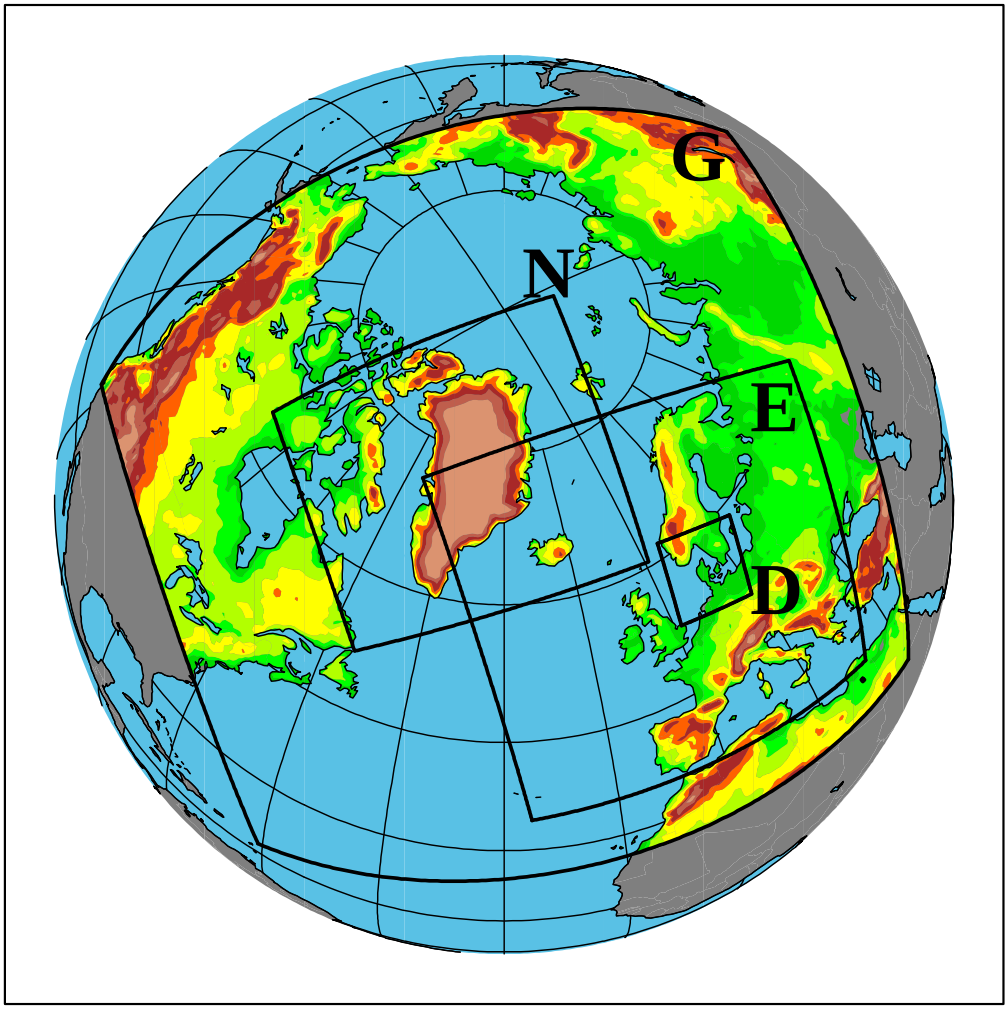

Figure 4: The DMI operational model integration areas.

the ECMWF (European Centre for Medium-Range Weather Forecasts) global model. Fresh boundaries are received 4 times a day as 'frames' covering the necessary boundary zone for coupling. The origin times of the boundary data is 00 UTC, 06 UTC, 12 UTC and 18 UTC, respectively. The horizontal resolution in this coupling zone equals the resolution of the 'G' model. In the vertical, every second level from the ECMWF model is used. In addition, the ECMWF sea surface temperature (SST) and fractional ice coverage are used on a daily basis, at a resolution of 1.0°, to update the corresponding fields in DMI-HIRLAM.

Table 1: Basic information related to model grid, resolution, time step, coupling strategy, forecast length and number of forecasts per day.

Model identification	G	N	E	D
grid points (mlon)	202	194	272	182
grid points (mlat)	190	210	282	170
number of vertical levels	31	31	31	31
horizontal resolution(deg)	0.45	0.15	0.15	0.05
resolution (assimilation)	0.45	0.45	0.45	-
time step (dynamics)	240 s	100 s	100 s	36 s
time step (physics)	720 s	600 s	600 s	216 s
host model	ECMWF	G	G	E
boundary age(forecast)	6 h	0 h	0 h	0 h
boundary age (assimilation)	0 h-6 h	−3 h - 0 h	−3 h - 0 h	−3 h - 0 h
boundary update cycle	3 h	1 h	1 h	1 h
data-assimilation cycle	3 h	3 h	3 h	3 h
forecast length (long)	60 h	36 h	54 h	36 h
long forecasts per day	4	2	4	2

The 'G' model provides the lateral boundary values of the models 'N' and 'E'. Finally, model 'E' supplies the boundaries for the very high resolution model 'D' around Denmark. The most important products from an operational point of view are produced by the high resolution models 'E', 'N' and 'D'.

The operational HIRLAM system is run on an NEC-SX4 supercomputer (analyses and forecasts), due to the need of a substantial computer power (see fig. 5).

The observation processing takes place on two 4 processor ORIGIN 200 computers. The GTS messages are processed and encoded to BUFR format. The SGI ORIGIN computers also contain an operational database with files produced by the operational runs. Some of the produced model level files are archived on a mass storage device.

Key parameters of the system setup with respect to resolution, time step, boundaries and data-assimilation are illustrated in table 1.

Here 'mlon' is the number longitude grid points and 'mlat' is the corresponding number of latitude points. For all operational models the geographical coordinates (polon, polat) of the rotated south pole are: (polon, polat) = $(80^\circ, 0^\circ)$.

Also the table shows the number of vertical levels in the models and the horizontal resolution (°) measured between neighboring grid points. Also the horizontal resolution used for the incremental variational data assimilation is given in the table (currently 0.45°) The time step used in the dynamics and in the physics are different, as mentioned in subsection 2.6. The boundary age means the age of the host model relative to the start time of the forecast. A distinction is made between boundary age dur-

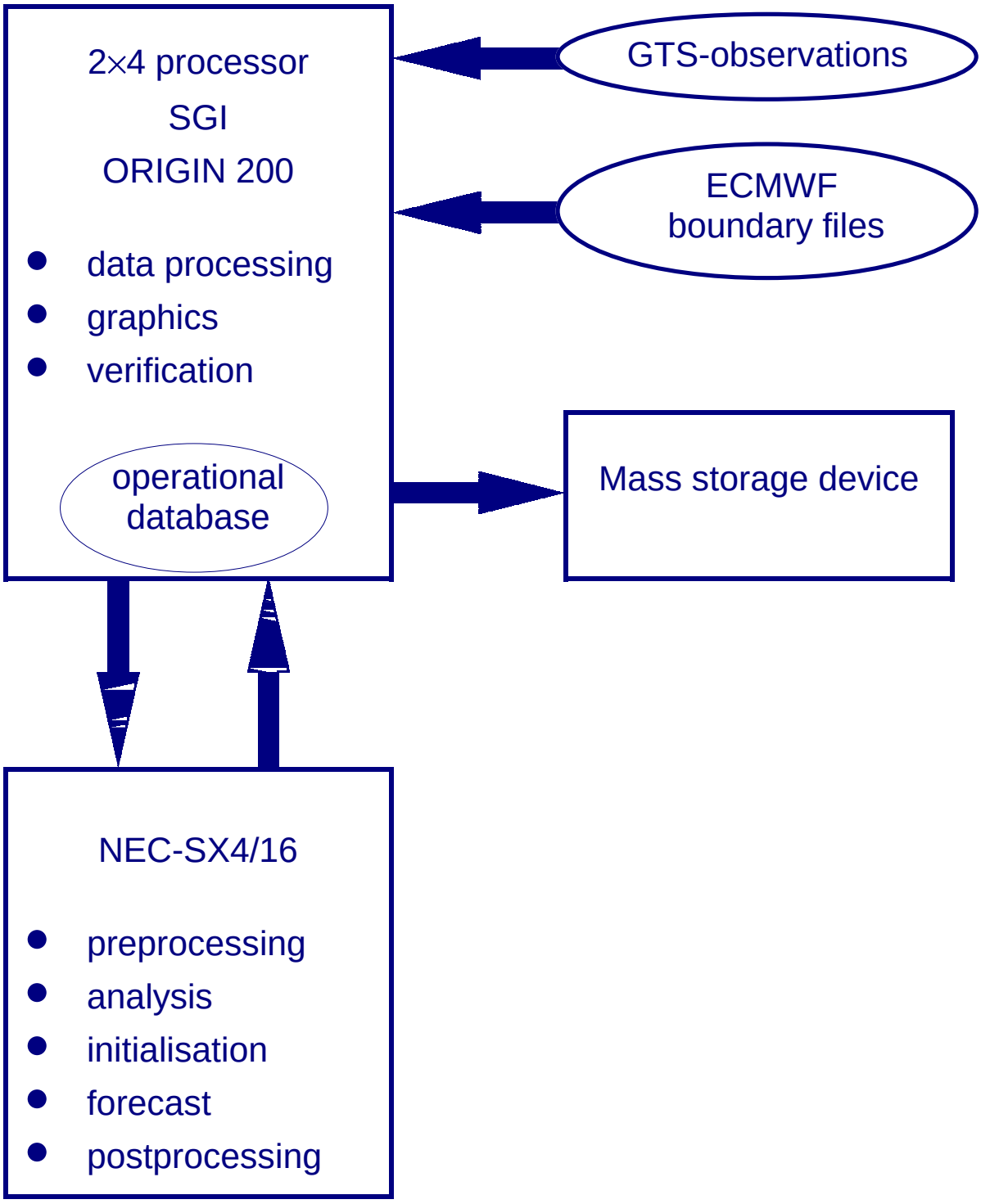

Figure 5: Computers and data flows.

ing forecast and during data-assimilation. A negative value of the boundary age during data-assimilation means that analyses of the host model are available and will be used as lateral boundaries. The boundary update cycle is given as the number of hours between boundary files of the host model used for time interpolation in boundary zone between the models. It is noted that output fields from the operational models are averaged over a period of approximately $\pm M.$ (depending on model time step), in order to assure that output will not be dominated by small scale features of very short duration. Currently $M = 7.5$ min. The data assimilation cycle is the number of hours between new analysis states of the model. Finally, the table provides information about the forecast length in hours and the number of long forecasts per day for each model.

The data-assimilation procedure is illustrated in table 2 showing the operational time schedule.

Variational data-assimilation (3D-Var) is implemented for all models except for model 'D' which makes use of analysis increments as described below.

The first column in table 2 indicates the model startup time in UTC. A given run is indicated by a letter followed by two digits describing model initial time, and finally an indication of forecast length in hours. For example, 'G00+60h' means a 00 UTC analysis followed by a 60 hour forecast carried out for model 'G'.

For the models 'G' and 'E' the initial states of the long forecasts are produced by analyses valid at 00 UTC, 06 UTC, 12 UTC and 18 UTC, respectively. A 6 hour forecast is used as input to these analysis states at 06 UTC and 18 UTC while a 3 hour forecast is the first guess input to other analyses.

For the models 'N' and 'D' long forecasts are run only two times a day on 00 UTC and 12 UTC initial time. A 3 hour forecast is input to these analyses.

The analysis states at 00 UTC and 12 UTC are achieved by retrospective analysis cycles twice a day. This means that the runs, with a cycling of 3 hours, are managed as a sequence of runs in delayed mode. The first series of runs starts around 11 UTC. Model 'G' starts from the 00 UTC ECMWF analysis data using an increment method where the available analysis for 'G' is interpolated to a mesh with coarser resolution ECMWF model data (a factor of 4 in resolution difference). The difference between this interpolated field and the new ECMWF analysis is an increment ('large scale increment') which is interpolated back to the HIRLAM field and added to get an updated HIRLAM analysis. Normal HIRLAM 3D-Var cycles then follow immediately after (analyses valid at 03 UTC, 06 UTC, 09 UTC) to produce an 'up-to-date' state of the atmosphere. The second series of runs is made in the evening, using 12 UTC ECMWF analysis data in the processing. These cycles produce 3D-Var analyses valid at 15 UTC, 18 UTC and 21 UTC respectively.

The analyses and forecasts produced in the assimilation cycles of model 'G' are used as boundaries for the corresponding 3-hourly cycles of the models 'E' and 'N'. These are also run as sequences in the late morning and in the evening. The boundary age during data assimilation cycles for these models is either 0 hours, or -3 hours if an analysed boundary from the host model ('G') is available.

An analysis increment method is also implemented for model 'D'. In this case the first guess of model 'D' is corrected using analyses from model 'E'. This method also applies to the 3-hourly cycles of model 'D'.

Table 2: Operational time schedule used (G_E denotes restart from ECMWF analysis. See text for details)

UTC	G	N	E	D
1:40	G00+60 h			
1:43			E00+54 h	
2:30				D00+36 h
2:55		N00+36 h		
ECMWF 00 UTC				
7:37	G06+60 h			
7:43			E06+54 h	
ECMWF 06 UTC				
11:50	G_E00+03 h G03+03 h G06+03 h G09+03 h			
12:00			E03+03 h E06+03 h E09+03 h	
12:10				D03+03 h D06+03 h D09+03 h
12:20		N03+03 h N06+03 h N06+03 h		
13:40	G12+60 h			
13:43			E12+54 h	
14:30				D12+36 h
14:55		N12+36 h		
ECMWF 12 UTC				
19:37	G18+60 h			
19:43			E18+54 h	
ECMWF 18 UTC				
23:45	G_E12+03 h G15+03 h G18+03 h G21+03 h			
23:55			E15+03 h E18+03 h E21+03 h	
24:05				D15+03 h D18+03 h D21+03 h
24:15		N15+03 h N18+03 h N21+03 h		

Appendix B. Grid used for horizontal discretization

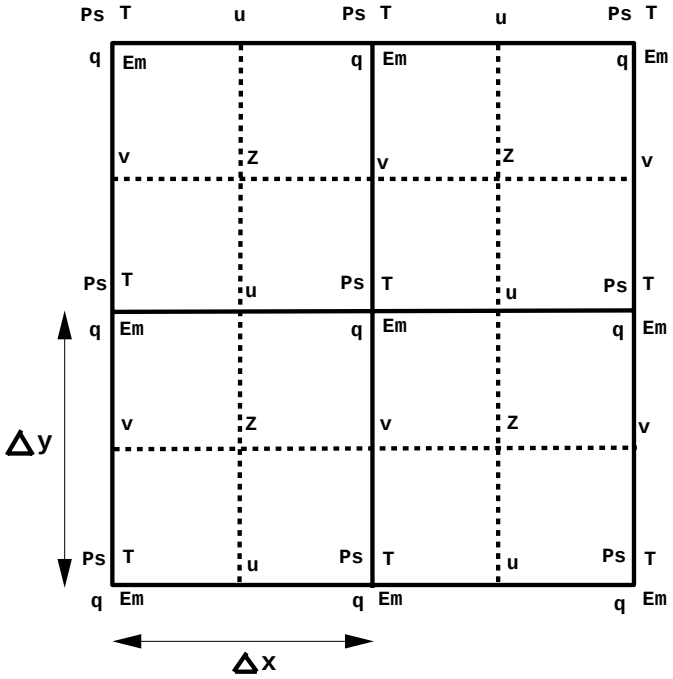

Figure 6: Arrangement of variables in Arakawa C grid. P_s is surface pressure, T is temperature, q is specific humidity (moisture variable), E_m is kinetic energy, u, v are horizontal wind components, Z is absolute vorticity.

Appendix B.1. Vertical coordinate levels

The vertical hybrid parameters used operationally $(A_{k+1/2}, B_{k+1/2})$ with $0 \leq k \leq N$. Currently the number of 'full' model levels N=31. The model 'half' levels are written below

$A_{k+1/2}$ =

0,2500,5000,7445.26,9890.52,12028.415,14166.31,15756.185,
17346.06,18233.605,19121.15,19246.195,19371.24,18767.855,18164.47,
16953.325,15742.18,14115.115,12488.05,10684.935,8881.82,7159.68,
5437.54,4031.9,2626.26,1704.78,783.3,391.65,0,0,0,0

$B_{k+1/2}$ =

0,0,0,0.00086,0.00172,0.00746,0.0132,0.02771,0.04222,0.06799,
0.09376,0.131665,0.16957,0.218795,0.26802,0.326145,0.38427,0.44755,
0.51083,0.57455,0.63827,0.697325,0.75638,0.805995,0.85561,0.89218,
0.92875,0.95087,0.97299,0.982635,0.99228,1

Appendix C. Computational details of longwave radiation

$$\left(\frac{\partial T}{\partial t}\right)_i = \left(\frac{\partial T}{\partial t}\right)_{i1a} + \left(\frac{\partial T}{\partial t}\right)_{i2a} + \left(\frac{\partial T}{\partial t}\right)_{i1c} + \left(\frac{\partial T}{\partial t}\right)_{i2c} \tag{112}$$

$$\left(\frac{\partial T}{\partial t}\right)_{i1a} = W_1(R_1 + R_2 + R_3) \tag{113}$$

$$\left(\frac{\partial T}{\partial t}\right)_{i2a} = W_2\zeta_2(R_1 + R_3) + (W_2 - W_3)R_2 \tag{114}$$

$$\left(\frac{\partial T}{\partial t}\right)_{i1c} = W_4R_4 + W_5R_5 + W_6R_6 \tag{115}$$

$$\left(\frac{\partial T}{\partial t}\right)_{i2c} = W_7R_7 + W_8R_5 + W_9R_6 \tag{116}$$

$R_1, \ldots, R_7$ are given in finite difference form below

$$R_1 = B(T_k)[e(0, p_{k-\frac{1}{2}}) - e(0, p_{k+\frac{1}{2}})]\frac{g}{c_p\Delta p_k}$$

$$R_2 = [B(T_{e0}) - B(T_k)][e(p_{k-\frac{1}{2}}, p_s) - e(p_{k+\frac{1}{2}}, p_s)]\frac{g}{c_p\Delta p_k}$$

$$R_3 = -a_6q_k^3 - a_7$$

$$R_4 = [-B(T_{k-\frac{1}{2}}) + B(T_{k-1})e(0, p_{k-\frac{1}{2}}) + a_9 - \zeta_3 + a_{10}\sqrt{q_{k-1}} + a_{11}q_{k-1}]\frac{g}{c_p\Delta p_k}$$

$$R_5 = [B(T_{l*}) - B(T_{k+\frac{1}{2}})][\zeta_4 + G_{k+1}(1 - \zeta_4)]\frac{g}{c_p\Delta p_k}$$

$$R_6 = [B(T_{e0}) - B(T_{k+\frac{1}{2}})][\zeta_5 + G_{k+1}(1 - \zeta_5)]\frac{g}{c_p\Delta p_k}$$

$$R_7 = [B(T_{h*}) - B(T_{k-\frac{1}{2}})][\zeta_6 + G_{k-1}(1 - \zeta_6)]\frac{g}{c_p\Delta p_k}$$

$$G_j = \frac{1}{1 + a_{13}\frac{(\Delta e)}{(\Delta p)_j}}, \quad 1 \le j \le N \tag{117}$$

The customary assumption is applied, that "grey" clouds may be introduced by reducing the normal grid box fractional cloud cover f with the cloud emissivity according to (118):

$$f_e = f[1 - \exp(-\zeta_1 M)] \tag{118}$$

The parameter ζ_1 depends on cloud type. It varies linearly with the vertical coordinate.

$$\zeta_1 = \max\left(0.05 + 0.20\frac{(\eta - \eta_1)}{1 - \eta_1}, 0.05\right), \quad \eta_1 = 0.25$$

M is the vertically integrated cloud condensate (g/m^2) in the cloud. The radiative impact of cloud layers above are taken into account by computing radiation from a maximum effective cloud cover f_{eh*}. In order to treat high vertical resolutions in a

realistic way this maximum effective cloud cover is determined in the following way: For any level above the layer in consideration and effective cloud cover is assigned by (118) using local values of cloud cover and ζ_1 while M is determined as the vertical integral of cloud condensate up to the top atmospheric model layer. The maximum of these effective cloud covers is f_{eh*} which is assigned to the level where the maximum occurs. A similar computation is carried out for the maximum effective cloud cover f_{el*} for clouds below the layer considered. Also the effect of the cloud covers f_{eh} and f_{el} of the neighboring layers above and below, respectively, is taken into account by assuming zero net flux contribution at the intersection of overlapping clouds.

$$\zeta_2 = \min\left(\frac{p_{k-\frac{1}{2}} - p_{h*}}{a_8}, 1\right)$$

$$\zeta_3 = a_{12}\frac{(1-\eta)}{(1-\eta_0)}, \quad \eta_0 = 0.05$$

$$\zeta_4 = \min\left(\frac{a_{14}}{p_{l*} - p_{k+\frac{1}{2}}}, 1\right)$$

$$\zeta_5 = \min\left(\frac{a_{14}}{p_s - p_{k+\frac{1}{2}}}, 1\right)$$

$$\zeta_6 = \min\left(\frac{a_{14}}{p_{k-\frac{1}{2}} - p_{h*}}, 1\right)$$

$B(T_j)$ is the Planck black body radiation at temperature T_j. R_1 is the "cooling to space" term, and R_2 accounts for the radiative effect of ground radiating with an effective temperature T_{e0}. The first term in R_3 represents crudely the effect of cooling due to water vapor continuum which is of major importance only in a moist and warm atmosphere (Savijärvi, 1990). The cooling due to other gases like CO_2 and O_3 seems to be rather small and fairly constant in the troposphere (Liou, 1980; Paltridge and Platt, 1976). Hence a constant cooling term a_7 is introduced to represent this.

The factor ζ_2 in (114) represents reduced cooling below clouds. Paltridge and Platt (1976) note that the assumption of zero cooling below clouds might be compatible with a "cooling to space" approximation. However, this assumption appears to be too drastic (Sass et al., 1994). Instead the cooling rate is assumed to vary linearly with a pressure increment below cloud, from zero to a value valid for 'clear air', through a certain depth a_8. The last term in (114) proportional to $W_2 - W_3$ represents the effect of radiation from the ground attenuated by overlapping low level clouds.

In (115) the first term estimates the net radiation balance at cloud top. The downward radiation due to gases other than water vapor including aerosols is described by $a_9 - \zeta_3$ taking into account a flux correction associated with the integrated cooling in clear air due to these constituents. The terms involving a_{10} and a_{11} parameterizes an additional flux due to water vapor continuum.

The additional terms in (115) and (116) involve a determination of effective radiation temperatures describing radiative interaction either between clouds or between ground and cloud. The first brackets in the formulations of R_5,R_6 and R_7 involving differences

between related Planck-functions is multiplied by a factor between 0 and 1 according to the expression in the second brackets. An empirical function G_j expressing sensitivity to the emissivity slope for clear air next to the cloud has been introduced (117). From a qualitative point of view it is obvious that the level of an effective radiation temperature for upward radiation comes closer to the ground as the humidity below cloud base decreases. In the extreme (unrealistic) situation of no absorption in the clear atmosphere the formulation automatically guarantees transmission of radiation between ground and cloud without attenuation.

$W_1, \ldots, W_9$ are weight functions related to the cloud overlap assumption.

$$W_1 = 1 - \max(f_e, f_{eh*})$$

$$W_2 = \max(f_{eh*} - f_e, 0)$$

$$W_3 = \min\left(\max(f_{el*} - f_e, 0.), W_2\right)$$

$$W_4 = \max(f_e - f_{eh*}, 0)$$

$$W_5 = \max\left(\min(f_{el*}, f_e) - f_{eh*}, 0\right) - \max\left(\min(f_{el}, f_e) - f_{eh*}, 0\right)$$

$$W_6 = W_4 - \max\left(\min(f_{el*}, f_e) - f_{eh*}, 0\right)$$

$$W_7 = \max\left(\min(f_{eh*}, f_e) - f_{eh}, 0.\right)$$

$$W_8 = \max\left(\min(\min(f_{el*}, f_e), f_{eh*}) - f_{el}, 0\right)$$

$$W_9 = \min(f_{eh*}, f_e) - \min\left(\min(f_{el*}, f_e), f_{eh*}\right)$$

Values of constants

$a_1 = 0.60$	$a_2 = 0.17$	$a_3 = 0.0082$
$a_4 = 0.0045$	$a_5 = 0.4343$	$a_6 = 11.5\ \frac{\mathrm{K}}{\mathrm{s}}$
$a_7 = 2.3{\cdot}10^{-6}\ \frac{\mathrm{K}}{\mathrm{s}}$	$a_8 = 7{\cdot}10^4\ \mathrm{Pa}$	$a_9 = 35\ \frac{\mathrm{J}}{\mathrm{m^2\,s}}$
$a_{10} = 250\ \frac{\mathrm{J}}{\mathrm{m^2\,s}}$	$a_{11} = 750\ \frac{\mathrm{J}}{\mathrm{m^2}}$	$a_{12} = 24\ \frac{\mathrm{J}}{\mathrm{m^2\,s}}$
$a_{13} = 2{\cdot}10^4\ \mathrm{Pa}$	$a_{14} = 2.5{\cdot}10^3\ \mathrm{Pa}$	$a_{15} = a_{14}$
$b_1 = 1.67$	$b_2 = 1.7{\cdot}10^{-6}\ \frac{\mathrm{K}}{\mathrm{s}}$	$b_3 = 0.03$
$b_4 = 0.05$	$b_5 = 1.20$	$b_6 = 1.25$
$b_7 = 0.013$	$b_8 = 1.4$	$b_9 = 0.10\ \frac{\mathrm{m^2}}{\mathrm{g}}$
$b_{10} = 40$	$b_{11} = 0.5$	$b_{12} = 0.8$

Stefan Boltzmann's constant $\sigma = 5.67{\cdot}10^{-8}\ \frac{\mathrm{J}}{\mathrm{m^2\,K^4\,s}}$

References

Andersson, E. and Järvinen, H. (1999). "Variational quality control.". *Q. J. R. Meteorol. Soc.* **125**: 697–722.

Arakawa, A. (1966). "Computational design for long-term numerical integration of the equations of fluid motion: twodimensional incompresible flow, part 1". *J. Comp. Phys.* **1**: 119–143.

Berre, L. (2000). "Estimation of synoptic and meso scale forecast error covariances in a limited area model.". *Mon. Wea. Rev.* **128**: 644–667.

Bister, M. (1998). "Cumulus Parameterisation in Regional Forecast Models: A Review". *HIRLAM Tech. Report* **35**: 1–32.

Brutsaert, W. (1975). "The Roughness Length for Water Vapor, Sensible Heat and Other Scalars". *J. Atmos. Sci.* **32**: 2028–2031.

Businger, J. A., Wyngaard, J. C., Izumi, Y., and Bradley, E. F. (1971). "Flux-Profile Relationships in the Atmospheric Surface Layer". *J. Atmos. Sci.* **28**: 181–189.

Charnock, H. (1955). "Wind stress on a water surface". *Quart. J. Roy. Meteorol. Soc.* **81**: 639–640.

Chou, M.-D. (1986). "Atmospheric Solar Heating Rate in the Water Vapor Bands". *J. Appl. Meteor.* **25**: 1532–1542.

Clayson, C. A., Fairall, C. W., and Curry, J. A. (1996). "Evaluation of turbulent fluxes at the ocean surface using surface renewal theory". *J. Geophys. Res.* **101**(C12): 28503–28513.

Cuxart, J., Bougeault, P., and Redelsperger, J.-L. (1995). "Turbulence closure for a non-hydrostatic model". In *12th AMS symp. on Boundary Layer Turbulence*, pages 409–412.

Cuxart, J., Bougeault, P., and Redelsperger, J.-L. (2000). "A turbulence scheme allowing for meso-scale and large-eddy simulations". *Quart. J. Roy. Meteorol. Soc.* **126**: 1–30.

Davies, H. C. (1976). "A lateral boundary formulation for multi-level prediction models". *Quart. J. Roy. Meteorol. Soc.* **102**: 405–418.

Deardorff, J. W. (1972). "Theoretical Expression for the Countergradient Vertical Heat Flux". *J. Geophys. Res.* **77**: 5900–5904.

DeCosmo, J., Katsaros, K. B., Smith, S. D., Anderson, R. J., Oost, W. A., Bumke, K., and Chadwick, H. (1996). "Air-sea exchange of water vapour and sensible heat: The Humidity Exchange Over the Sea (HEXOS) results". *J. Geophys. Res.* **101**(C5): 12001–12016.

Emanuel, K. A. (1991). "A Scheme for Representing Cumulus Convection in Large-Scale Models". *J. Atmos. Sci.* **48**: 2313–2335.

Garrat, J. R. (1977). "Review of Drag Coefficients over Oceans and Continents". *Mon. Weather Rev.* **105**: 915–929.

Garrat, J. R. (1992). *The Atmospheric Boundary Layer.* Cambridge University Press.

Grachev, A. A., Fairall, C. W., and Larsen, S. E. (1998). "On the determination of the neutral drag coefficient in the convective boundary layer". *Boundary-Layer Meteorol.* **86**: 257–278.

Gustafsson, N. (1993). "The HIRLAM 2 Final Report". *HIRLAM Tech. Report* **9**.

Gustafsson, N., Berre, L., Hörnquist, S., Huang, X.-Y., Lindskog, M., Navascués, B., Mogensen, K. S., and Thorsteinsson, S. (2001). "Three-dimensional variational data-assimilation for a limited area model. Part I: General formulation and the background error constraint". *Tellus* **53A**: 425–446.

Haltiner, G. J. (1971). *Numerical Weather Prediction.* J. Wiley & Sons.

Hansen, C. and Larsen, S. E. (1997). "Further Work on the Kitaigorodskii Roughness Length Model: A New Derivation Using Lettau's Expression on Steep Waves". *Geophysica* **33**(2): 29–44.

Holtslag, A. A. M. and Boville, B. A. (1993). "Local versus nonlocal boundary layer diffusion in a global climate model layer". *J. Climate* **6**: 1825–1842.

Kållberg, P. (1977). "Test of a boundary relaxation scheme in a barotropic model". *ECMWF research department internal report* **3**: 1–21.

Källén, E. (1996). "HIRLAM Documentation Manual. System 2.5". *SMHI, Norrköping, Sweden.*

Kalnay, E. and Kanamitsu, M. (1988). "Time Schemes for Strongly Nonlinear Damping Equations". *Mon. Weather Rev.* **116**: 1945–1958.

Krayer, W. and Marshall, R. (1992). "Gust factors applied to hurricane winds". *Bull. Am. Met. Soc.* **73**: 613–617.

Kunkel (1984). "Parameterization of droplet terminal velocity and extinction coefficient in fog models". *J. Climate Appl. Meteor.* **23**: 34–41.

Kuo, H. L. (1974). "Further Studies of the Parameterization of the Influence of Cumulus Convection on Large-Scale Flow". *J. Atmos. Sci.* **31**: 1232–1240.

Lindskog, M., Gustafsson, N., Navascués, B., Mogensen, K. S., Huang, X.-Y., Yang, X., , Andræ, U., berre, L., Thorsteinsson, S., and Rantakokko, J. (2001). "Three-dimensional variational data-assimilation for a limited area model. Part II: Observation handling and assimilation experiments". *Tellus* **53A**: 447–468.

Liou, K. N. (1980). *An Introduction to Atmospheric Radiation.* Academic Press.

Liou, K.-N. and Wittman, G. D. (1979). "Parameterization of the Radiative Properties of Clouds". *J. Atmos. Sci.* **36**: 1261–1273.

Liu, W. T., Katsaros, K. B., and Businger, J. A. (1979). "Bulk Parameterization of Air-Sea Interaction of Heat and Water Vapor Including the Molecular Constraints at the Interface". *J. Atmos. Sci.* **36**: 1722–1735.

Lorenc, A. and Hammon, O. (1988). "Objective quality control of observations using Bayesian methods. Theory and practical implementation.". *Quart. J. Roy. Meteorol. Soc.* **114**: 515–543.

Lorenc, A. C. (1986). "Analysis methods for numerical weather prediction". *Quart. J. Roy. Meteorol. Soc.* **112**: 1177–1194.

Louis, J.-F. (1979). "A parametric model of vertical eddy fluxes in the atmosphere". *Boundary-Layer Meteorol.* **17**: 187–202.

Louis, J. F., Tiedtke, M., and Geleyn, J. F. (1982). "A short history of the operational PBL parameterization at ECMWF". In *Workshop on Boundary Layer Parameterization*, pages 59–79, ECMWF, Reading.

Maat, N., Kraan, C., and Oost, W. A. (1991). "The roughness of wind waves". *Boundary-Layer Meteorol.* **54**: 89–103.

Machenhauer, B. (1988). "HIRLAM Final Report". *HIRLAM Tech. Report* **5**: 1–116.

McDonald, A. (1998). "The origin of noise in semi-Lagrangian integrations". Met Eireann Tech. Note 55, Met Eireann.

Mogensen, K. S., Jørgensen, J. U., Amstrup, B., Yang, X., and Huang, X.-Y. (2000). "Results of the pre-operational HIRLAM 3D-VAR runs at DMI". *HIRLAM Newsletter* **36**: 6–15.

Nielsen, N. W. (1998). "The first order nonlocal vertical diffusion scheme in HIRLAM 4.1". *HIRLAM Newsletter* **31**: 12–13.

Nielsen, N. W. (1999). "A revised formulation of surface fluxes over sea". In *HIRLAM 4 Workshop on Physical Parameterization, Madrid, 11-13 November 1998*, pages 112–120.

Nielsen, N. W. and Petersen, C. (2001). "Calculation of wind gusts in DMI-HIRLAM". *DMI Sci. Rep. 01-03* pages 1–32.

Olofsson, B., Andersson, S., Mårtensson, T., Mårtensson, E., and Olsson, E. (1999). "Projekt Isbildningsprognoser". Swedish defense administration report, Försvarsmakten, Stockholm, Sweden.

Oost, W. A. (1998). "The KNMI HEXMAX Stress Data–A Reanalysis". *Boundary-Layer Meteorol.* **86**: 447–468.

Paltridge, P. W. and Platt, C. M. R. (1976). *Radiative processes in Meteorology and Climatology.* Elsevier Scientific Publishing Company.

Parrish, D. F. and Derber, J. (1992). "The National Meteorological Center's spectral statistical interpolation analysis system". *Mon. Wea. Rev.* **120**: 1747–1763.

Paulson, C. A. (1970). "The Mathematical Representation of Wind Speed and Temperature Profiles in the Unstable Atmospheric Surface Layer". *J. Appl. Meteor.* **9**: 857–861.

Petersen, C. and Nielsen, N. W. (2000). "Diagnosis of visibility in DMI-HIRLAM". DMI scientific report no. 00-11, Danish Meteorological Institute, Copenhagen Denmark.

Pielke, R. A. and Cram, J. M. (1987). "An Alternate Procedure for Analyzing Surface Geostrophic Winds and Pressure over Elevated Terrain". *Weather and forecasting* **2**: 229–236.

Rabier, F., McNally, A., Andersson, E., Courtier, P., Undén, P., Eyre, J., Hollingswoth, A., and Bouttier, F. (1998). "The ECMWF implementation of three-dimensional data-assimilation 3D-Var, part II: Structure functions.". *Quart. J. Roy. Meteorol. Soc.* **124**: 1809–1830.

Redelsperger, J. L. and Sommeria, G. (1986). "Three-Dimensional Simulation of a Convective Storm: Sensitivity Studies on Subgrid Parameterization and Spatial Resolution". *J. Atmos. Sci.* **43**: 2619–2635.

Sadourny, R. (1975). "The Dynamics of Finite-Difference Models of the Shallow-Water Equations". *J. Atmos. Sci.* **32**: 680–689.

Sasamori, T., London, J., and Hoyt, D. V. (1972). "Radiation budget of the Southern Hemisphere". *Meteor. Monogr.* **13**(35): 9–23.

Sass, B. (2001). "Modelling of the time evolution of low tropospheric clouds capped by a stable layer". *HIRLAM Tech. Report* **50**: 1–43.

Sass, B. H. (1999). "Implicit treatment of turbulent kinetic energy dissipation in the CBR turbulence scheme". *HIRLAM Newsletter* **34**: 43–51.

Sass, B. H., Rontu, L., and Räisänen, P. (1994). "HIRLAM-2 Radiation Scheme: Documentation and Tests". *HIRLAM Tech. Report* **16**: 1–43.

Sattler, K. (1999). "New high resolution physiographic data and climate generation for the HIRLAM forecasting system". Tech. report 99-11, Danish Meteorological Institute.

Savijärvi, H. (1990). "Fast Radiation Parameterization Schemes for Mesoscale and Short-Range Forecast Models". *J. Appl. Meteor.* **29**: 437–447.

Simmons, A. J. and Burridge, D. M. (1981). "An Energy and Angular-Momentum Conserving Vertical Finite-Difference Scheme and Hybrid Vertical Coordinates". *Mon. Weather Rev.* **109**: 758–766.

Slingo, A., Nicholls, S., and Schmetz, J. (1982). "Aircraft observations of marine stratoculumus during JASIN". *Quart. J. Roy. Meteorol. Soc.* **108**: 833–856.

Stephens, G. L. (1978). "Radiation Profiles in Extended Water Clouds. I: Theory". *J. Atmos. Sci.* **35**: 2111–2122.

Sundqvist, H. (1993). "Inclusion of Ice Phase of Hydrometeors in Cloud Parameterization for Mesoscale and Largescale Models". *Beitr. Phys. Atmosph./Contrib. Atmos. Phys.* **66**: 137–147.

Sundqvist, H., Berge, E., and Kristjánsson, J. E. (1989). "Condensation and Cloud Parameterization Studies with a Mesoscale Numerical Weather Prediction Model". *Mon. Weather Rev.* **117**: 1641–1657.

Tiedtke, M. (1993). "Representation of Clouds in Large-Scale Models". *Mon. Weather Rev.* **121**: 3040–3061.

Undén, P., Rontu, L., Calvo, J., Cats, G., Cuxart, J., Eerola, K., Fortelius, C., Garcia-Moya, J. A., Gustafsson, N., Jones, C., Järvenoja, S., Järvinen, H., Lynch, P., McDonald, A., MsGrath, R., Nvascues, B., Odegaard, V., Rodriguez, E., Rummukainen, M., Rõõm, R., Sattler, K., Savijärvi, H., Sass, B. H., Schreur, B. W., The, H., and Tijm, S. (2002). "The HIRLAM-5 Scientific Documentation". HIRLAM-5 project, SMHI Norrköping, Sweden.

Vogelezang, D. H. P. and Holtslag, A. A. M. (1996). "Evaluation and model impacts of alternative boundary-layer height formulations". *Boundary-Layer Meteorol.* **81**: 245–269.

Wedi, N. P. (1999a). "The numerical coupling of the physical parametrizations to the dynamical equations in a forecast model". *ECMWF Technical Memorandum* **274**.

Wedi, N. P. (1999b). "Recent Developments at ECMWF. Numerics and Resolution". *LAM Newsletter* **28**: 43–47. (available from DMI).

Yelland, M. and Taylor, T. K. (1996). "Wind stress measurements from the open ocean". *J. Phys. Oceanog.* **26**: 541–558.

Index

absorption
  cloud, 16
aircraft
  icing index, 39
Arakawa C grid, *see* grid

boundary conditions, 8
boundary layer height, 37
buoyancy, 20, 22

Charnock formula, 29
climate
  deep soil temperature, 30, 31
cloud
  absorption, 16
cloud condensate, 23, 33
  specific, 5
cloud cover, 38
  convective, 25
  stratiform, 26
cloud water, 15, 17
  specific, 20
CMA, 34
coefficient
  diffusion, 8
  drag, 27
  eddy exchange, 20
coefficients
  $A_{k+\frac{1}{2}}$, 7, 47
  $B_{k+\frac{1}{2}}$, 7, 47
  $\eta_{k+\frac{1}{2}}$, 7
condition
  boundary, 8
constant
  von Kármán, 27
continuity
  equation, 6
convection
  shallow, 23
convection scheme
  STRACO, 23
coordinate surface
  half level, 7
coordinates
  pressure, 7
  spherical rotated, 5
  terrain following, 5, 7
    η, 5

deep soil temperature
  climate, 30, 31
δ_c, 6
diffusion
  coefficient, 8
diffusion scheme
  turbulent kinetic energy, 14
divergence operator, 6
drag
  force, 29
drag coefficient, 27
dynamics
  Eulerian, 9

ECMWF, 3
eddy exchange coefficient, 20
emissivity function, 17
energy
  turbulent kinetic, 5
equation
  continuity, 6
  hydrostatic, 6
  momentum, 5
η, 5
Eulerian
  dynamics, 9

fog, 38
formula
  Charnock, 29

GCSS, 23
geopotential, 6
GEWEX, 23
GLCC, 32
gravity
  wave drag, 14
grid
  Arakawa C, 7, 47
GTOPO30, 32

half levels, 7
height
    boundary layer, 37
HIRLAM, 3
    convection schemes, 23
    DMI operational system, 41
    model mesh size, 13
    physiographic data, 32
HIRVDA, 34
horizontal diffusion scheme, 8
humidity
    specific, 21, 25, 36
    surface specific, 27
hydrostatic
    equation, 6

icing index, 39

κ, 6
kinetic energy
    subgrid scale, 19, 20
    turbulent, 5, 6, 14

LAM, 8
leapfrog time step, 7
longwave scheme, 17
Louis scheme, 19

momentum
    equation, 5
Monin-Obukov length scale, 21

number
    Redelsperger, 21
    Richardson, 28, 37

observations
    AIREP, 35
    AMDAR/ACARS, 35
    DRIBU, 35
    SHIP, 35
    SYNOP, 35
    TEMP, 35
OBSPROC, 34
operator
    divergence, 6
orography
    subgrid scale, 14, 28

physiographic
    data, 14
physiographic data
    HIRLAM, 32
potential temperature, *see* temperature
pressure
    vertical velocity, 6
prognostic variable
    cloud condensate, 23
prognostic variables, 8

radiation
    computational details, 48
    longwave, 17
    scheme, 15
    solar, 15
    thermal, 15
Redelsperger number, 21
Reynolds number
    roughness, 29
Reynolds terms, 20
Richardson number, 28, 37
roughness
    length, 28

scheme
    fast radiation, 15
    horizontal diffusion, 8
    longwave, 17
    Louis, 19
    semi-implicit, 8
semi-implicit scheme, 8
shallow convection, 23
soil moisture, 30
soil water, 31
specific cloud water, 20
specific heat capacity
    soil, 31
STRACO, 23
surface
    pressure tendency, 6

temperature
    2 m, 36
    equation, 6
    potential, 20, 36
temperature tendency

radiative, 18
time
filter, 9
time step
leapfrog, 7
time stepping, 9
transport
vertical, 19

USGS, 14

variables
forecast, 5
prognostic, 8
vertical
transport, 19
vertical velocity
pressure, 6
visibility, 38
von Kármán constant, 27
vorticity, 6

wind
gusts, 39